HHS Public Access

Author manuscript

Neuron. Author manuscript; available in PMC 2018 May 03.

Published in final edited form as:

Neuron. 2017 May 03; 94(3): 595–610.e6. doi:10.1016/j.neuron.2017.04.004.

Releasing Syntaphilin Removes Stressed Mitochondria from Axons Independent of Mitophagy under Pathophysiological Conditions

Mei-Yao Lin[1,*], **Xiu-Tang Cheng**[1,*], **Prasad Tammineni**[2], **Yuxiang Xie**[1], **Bing Zhou**[1], **Qian Cai**[2], and **Zu-Hang Sheng**[1,#]

[1]Synaptic Function Section, The Porter Neuroscience Research Center, National Institute of Neurological Disorders and Stroke, National Institutes of Health, Room 2B-215, 35 Convent Drive, Bethesda, Maryland 20892-3706, USA

[2]Department of Cell Biology and Neuroscience, Rutgers, The State University of New Jersey, Piscataway, NJ 08854, USA

Abstract

Chronic mitochondrial stress is a central problem associated with neurodegenerative diseases. Early removal of defective mitochondria from axons constitutes a critical step of mitochondrial quality control. Here we investigate axonal mitochondrial response to mild stress in wild-type neurons and chronic mitochondrial defects in Amytrophic Lateral Sclerosis (ALS)- and Alzheimer's disease (AD)-linked neurons. We show that stressed mitochondria are removed from axons triggered by the bulk release of mitochondrial anchoring protein syntaphilin via a new class of mitochondria-derived cargos independent of Parkin, Drp1 and autophagy. Immuno-electron microscopy and super-resolution imaging show the budding of syntaphilin cargos, which then share a ride on late endosomes for transport toward the soma. Releasing syntaphilin is also activated in the early pathological stages of ALS- and AD-linked mutant neurons. Our study provides new mechanistic insights into the maintenance of axonal mitochondrial quality through SNPH-mediated coordination of mitochondrial stress and motility before activation of Parkin-mediated mitophagy.

eTOC Blurb

[#]Correspondence and Lead contact: Z.-H. Sheng (shengz@ninds.nih.gov).
[*]These authors contributed equally to this work

Author Contributions:

M-Y. L and X-T. C designed and conducted cell biology experiments and data analysis; Y. X and B. Z characterized ALS neurons; P. T and Q. C characterized AD neurons; Z.-H. S is the senior author who conceived and designed the project; M-Y. L, X-T. C, Q. C. and Z-H. S. wrote the manuscript.

COMPETING INTERESTS STATMENT

The authors declare no competing financial interests.

Lin and Cheng et al. reveal a new mechanism maintaining axonal mitochondrial integrity by releasing anchoring protein syntaphilin from stressed mitochondria, thus facilitating the removal of dysfunctional mitochondria from axons before activation of Parkin-mediated mitophagy under physiological and pathological conditions.

Keywords

Mitochondrial quality control; axonal mitochondria; mitochondrial transport; physiological stress; syntaphilin; AD; ALS; late endosome

Introduction

Mitochondria supply cellular energy and maintain Ca^{2+} homeostasis essential for neuronal survival and function (Chen and Chan, 2009; Sheng and Cai, 2012). Neurons are highly polarized cells with an extended axon, thus facing the special challenge of maintaining mitochondrial integrity and energy homeostasis. Mitochondria undergo long-distance transport to growth cones and presynaptic terminals to meet high metabolic demands. In addition, a mitochondrion ages in a few weeks and is dysfunctional under stress conditions when its integrity is impaired (Cai et al., 2012; Chang and Reynolds, 2006; Miller and Sheetz, 2004). Distal mitochondria often contain more aged proteins than those located in the proximal regions of neurons (Ferree et al., 2013). Chronic mitochondrial stress and impaired transport have been implicated in major neurodegenerative diseases including AD and ALS (De Vos et al., 2007; Wong et al., 1995; Vande Velde et al., 2011; Xie et al., 2015). Long-term cumulative stress leads to axonal accumulation of damaged mitochondria that not only produce energy less efficiently, but also release harmful reactive oxygen species. Therefore, the early removal of defective mitochondria from axons constitutes a critical step of mitochondrial quality control. However, the underlying mechanisms have yet to be elucidated.

PINK1/Parkin pathway has been well characterized as the key mechanism of mitochondrial quality control (Narendra et al., 2008). However, primary neurons often show delayed Parkin-mediated mitophagy in response to depolarization of mitochondrial membrane potentials ($\Delta\psi_m$) (Van Laar et al., 2011; Cai et al., 2012), raising the question of whether mitophagy is an early quality control mechanism for neuronal mitochondria. Acute mitochondrial depolarization with a high-dose of Antimycin A1 (AA, 40 μM), a respiratory complex III inhibitor, quickly induces Parkin-mediated mitophagy in axons within ~50 minutes (Ashrafi et al., 2014). However, it is not known whether axonal mitophagy could be induced by mild and chronic mitochondrial stress, a condition more relevant to chronic and progressive mitochondrial dysfunction in several major neurodegenerative diseases. It also remains unclear whether other mechanisms play an early role in the maintenance of axonal mitochondrial quality before the activation of Parkin-mediated mitophagy. Recent studies with genetic PINK1 and Parkin mutations support the model that mitochondrial turnover is mainly restricted to the soma in the *Drosophila* nervous system *in vivo* (Devireddy et al., 2015; Sung et al., 2016), thus calling for investigations into how damaged mitochondria are removed from axons under pathophysiological conditions.

Kinesin and cytoplasmic dynein motors drive axonal mitochondria for anterograde and retrograde transport, respectively (Birsa et al., 2013; Saxton and Hollenbeck, 2012; Schwarz, 2013; Sheng, 2014, 2017). Our previous studies identified syntaphilin (SNPH) as a static anchor that immobilizes axonal mitochondria through its mitochondria-targeting sequence and microtubule-anchoring domain (Chen et al., 2013; Kang et al., 2008). Deleting murine *snph* substantially increases the percentage of motile axonal mitochondria, while over-expressing SNPH abolishes axonal mitochondrial transport (Zhou et al., 2016). Motors and SNPH play opposite roles in regulating mitochondrial motility in axons (van Bergeijk et al., 2015). Releasing SNPH from mitochondria would thus shift the balance between motor-driven trafficking and SNPH-mediated anchoring. Interestingly, SNPH expression is strictly regulated during brain development. Decline in mitochondrial transport in mature neurons correlates with increased levels of SNPH expression (Zhou et al., 2016). The SNPH expression pattern allows us to propose a hypothesis: mature neurons have an intrinsic mechanism removing stressed mitochondria that are anchored in distal axons by selective degradation of SNPH when mitochondria are under stress conditions in healthy and diseased neurons.

Here, we investigate the early response of axonal mitochondria to a mild mitochondrial stress in wild-type (WT) neurons and chronic pathological stress in ALS- and AD-linked neurons. We demonstrate that mitochondrial transport is critical for maintaining their integrity. The selective bulk release of SNPH from stressed mitochondria enhances mitochondrial transport long before Parkin-mediated mitophagy is activated. This process is robustly activated during the early disease stages of hALS-linked spinal motor neurons and AD-related cortical neurons. Our study reveals a new mechanism for the maintenance of axonal mitochondrial integrity through the down-regulation of syntaphilin-mediated anchoring of mildly damaged mitochondria as an early stress response, facilitating mitochondrial turnover or recovery in the cell body under physiological and pathological conditions. Our findings thus benefit the development of new strategies to attenuate chronic mitochondrial pathology associated with major neurodegenerative diseases early in disease progression.

RESULTS

Inducing Mild Stress to Mitochondrial without Activating Parkin-Mediated Mitophagy

Acute depolarization of mitochondria with high doses (μM) of the $\Delta\psi_m$ un-coupler carbonyl cyanide 3-cholorophenylhydrazone (CCCP) or the respiratory complex III inhibitor AA has been widely used to study mitochondrial quality control in cultured cells. These approaches, however, prevent investigation into the early-stage of mitochondrial quality control in neurons under mild and chronic stress conditions (Schon and Przedborski, 2011). Mitochondrial $\Delta\psi_m$, generated by oxidative phosphorylation through the electron transport chain, drives ATP production. To induce a mild and reversible mitochondrial stress, we used the Seahorse XFe analyzer to examine the oxygen consumption rate (OCR) following AA treatment with various dosages and durations. AA blocks electron transport complex III, leading to a depolarization of $\Delta\psi_m$ and a rapid decrease in O_2 consumption. Thus, OCR is a sensitive readout for AA-induced mitochondrial dysfunction. Cortical neurons were treated

with three concentrations of AA (5 nM, 100 nM, and 10 μM) for various time periods plus a 1-hour recovery following the 6-hour AA treatment. Acute treatment with a high-dose AA (100 nM or 10 μM) causes a dramatic reduction of OCR from 8.15 ± 0.12 to 1.94 ± 0.13 (p<0.0001) or 1.45 ± 0.09 (p<0.0001) (pmole/min/μg protein), respectively, within 30 minutes. In contrast, a low-dose AA (5 nM) gradually reduces mitochondrial OCR when the treatment prolongs to 6 hours. Such a delayed reduction could be partially reversed after removing AA from the medium for 1 hour (Figure 1A). However, the OCR recovery is not observed under a high-dose AA treatment (100 nM or 10 μM). Thus, we justified that the treatment of neurons with 5 nM AA for 6 hours induces slow and reversible mild mitochondrial stress. We next confirmed whether this mild AA treatment depolarizes mitochondria in hippocampal neurons expressing GFP-Mito, a green fluorescent protein targeting the mitochondrial matrix. Following AA treatment (5 nM) for 6 hours, neurons were loaded with a $\Delta\psi_m$-dependent dye TMRE. The majority of mitochondria in both somatodendritic regions and distal axons lose TMRE staining (Figures S1A, S1B), suggesting that such a mild stress is sufficient to induce mitochondrial depolarization in live neurons. Given that acute neuronal mitophagy has been well characterized (Ashrafi et al., 2014), we instead study the mechanisms maintaining axonal mitochondrial integrity in response to mild and reversible stress that is more relevant to chronic mitochondrial dysfunction associated with several aging-related neurodegenerative diseases.

Our previous study using well-maintained mature cortical neurons demonstrates that the translocation of cytosolic Parkin into depolarized mitochondria occurs mainly in the somatic regions after 24-hour CCCP (10 μM) treatment (Cai et al., 2012). We speculate that Parkin-mediated mitophagy unlikely occurs under mild stress conditions. To confirm this, we over-expressed GFP-Parkin and DsRed-Mito in hippocampal neurons followed by 5 nM AA treatment at DIV10. Parkin-targeted mitophagosomes within the soma are quickly eliminated in lysosomes over a time course of ~25 minutes (Cai et al., 2012), we added lysosomal inhibitors (LIs) 1 hour prior to AA treatment to prevent the degradation of mitophagy during prolonged AA treatment. After 6-hour AA treatment, we detected no Parkin translocation to mitochondria either in the soma or neurites (Figure S1C). Only with a prolonged treatment to 30 and 48 hours, Parkin translocation gradually occurs but is mainly found in the soma and proximal regions. We next performed line scan analysis of the co-localization of Parkin and mitochondria along axons. A Parkin-targeted mitochondrion was considered when the relative intensity of GFP-Parkin peak was at least twice that of the neighboring peaks (Ashrafi et al., 2014). We found no detectable Parkin-targeted mitochondria in axons following mild AA treatment (5 nM) for 6 hours. After a 36-hour prolonged treatment, only a small population (3.62 ± 0.45%) of axonal mitochondria displays Parkin translocation (Figures S1D, S1E). While an acute depolarization triggers Parkin-mediated mitophagy in axons (Ashrafi et al., 2014), mild mitochondrial stress may involve alternative mechanisms that maintain axonal mitochondrial quality before Parkin-mediated mitophagy is activated.

Mitochondrial Transport Maintains Axonal Mitochondrial Integrity Under Mild Stress

Delayed Parkin-mediated mitophagy raises a fundamental question as to whether neurons have unique mechanisms maintaining distal mitochondrial integrity under physiological and

pathological stress conditions. Instead of globally depolarizing mitochondria in culture dishes, we sought to spatiotemporally depolarize mitochondria within distal axons by applying a microfluidic chamber (Figure 1B). Expressing the mitochondria-anchoring protein SNPH reduces the mitochondrial flux rate along axons in microgrooves ($p<0.001$) relative to control neurons (Figure 1C left panels). In contrast, expressing a HA-tagged mitochondrial motor adaptor complex protein Miro1 (HA-Miro1) significantly enhances the mitochondrial flux rate ($p<0.001$). Axonal mitochondria were depolarized at DIV8 by loading 5 nM AA into the axonal chamber for 3 or 6 hours. Loss of $\Delta\psi_m$ was confirmed by loading 100 nM MitoTracker CMTMRos (CMTMRos), a fixable $\Delta\psi_m$-dependent dye. The impact of mitochondrial transport on the maintenance of mitochondrial integrity was assessed 1 hour after removing AA from the axonal chamber. A partial recovery of axonal mitochondria $\Delta\psi_m$ was observed in control neurons (Figure S2A). The neurons with enhanced mitochondrial motility by expressing HA-Miro1 display a greater recovery of mitochondrial $\Delta\psi_m$ than neurons expressing control HA ($p<0.0001$). In contrast, arresting mitochondrial transport by overexpressing HA-SNPH impairs such recovery ($p<0.0001$) (Figures S2A, 1C, 1D). Mitochondria in the somatic chamber retain their CMTMRos staining following a 6-hour AA treatment in axonal chamber (Figures S2B, S2C), suggesting the fluidic isolation of AA and restricted depolarization of axonal mitochondria. In addition, the enhanced mitochondrial transport in the *snph* knockout (KO) neurons significantly improves the maintenance of axonal mitochondrial $\Delta\psi_m$ when compared to WT neurons ($p<0.0001$) following the axon-restricted application of 5 nM AA for 6 hours (Figure S2D).

We next asked whether mitochondrial transport is critical for the maintenance of axonal mitochondrial integrity in response to chronic pathological stress. We applied adult DRG neurons isolated from postnatal day 40 (P40) $hSOD1^{G93A}$ mice in the early disease stages (Xie et al., 2015). Arresting mitochondrial transport by overexpressing SNPH impairs the maintenance of axonal mitochondrial integrity ($p=0.034$) (Figure 1E). However, in age-matched WT neurons axonal mitochondrial $\Delta\psi_m$ is maintained following SNPH expression if no stress is induced. This result suggests that neurons with pathological burden are more vulnerable to an impaired mitochondrial transport. Thus, proper mitochondrial motility is critical to maintaining axonal mitochondrial quality under both mild mitochondrial stress and chronic pathological conditions.

We next asked how mitochondrial quality control is achieved under mild stress conditions through the regulation of axonal mitochondrial motility. DRG neurons provide an ideal cell model for studying axonal transport because almost all neurites are tau-positive axons (Perlson et al., 2009). DRG neurons transfected with GFP-Mito at DIV0 were treated with 5 nM AA for 6 hours and then recovered for 1 hour at DIV3, followed by a 20-min of TMRE staining. 82.08 ± 3.99% of TMRE-labeled polarized mitochondria move in an anterograde direction toward distal ends while 78.44 ± 5.27% of TMRE-negative depolarized mitochondria move retrogradely toward the soma. (Figure 1F). These results suggest that neurons may utilize a specialized mechanism for mitochondrial quality control through selective bi-directional transport, thus removing stressed mitochondria from and replenishing healthy ones to distal axons. Our findings are recapitulated in the intact *in vivo* nervous system where mitochondrial turnover is mainly found to the soma (Devireddy et al., 2015; Sung et al., 2016). Impaired mitochondrial transport associated with major

neurodegenerative diseases likely contributes to the long-term accumulative effects that lead to mitochondrial pathology in distal axons.

Enhanced Transport Is Triggered by Releasing SNPH from Stressed Mitochondria

To understand how axonal mitochondrial stress and their motility are coordinated, we characterized mitochondrial transport following varying durations of AA treatment. In contrast to the report showing arrested mitochondrial transport by acute high-dose AA treatment (Ashrafi et al., 2014), axonal mitochondria remain highly motile under mild stress conditions. The 6-hour AA treatment (5 nM) enhances retrograde transport from 17.42 ± 1.30% to 33.04 ± 2.20% (p<0.0001) (Figures 2A, 2B, Movies S1–S4). However, the same AA treatment is unable to enhance retrograde transport in the *snph* KO neurons (Figures 2C, 2D), indicating a critical role of SNPH in the stress-induced regulation of axonal mitochondrial transport. Next, we examined SNPH levels in cortical neurons under mitochondrial mild stress conditions. SNPH, but not other outer mitochondrial membrane (OMM) proteins Miro1, TOM20, and VDAC, is selectively reduced as early as 6 hours of 5 nM AA treatment (Figures 2E, 2F).

To confirm the reduction of SNPH on axonal mitochondria, we co-immunostained neurons with antibodies against cytochrome c and SNPH or TOM20. To our surprise, mild mitochondrial stress induces SNPH redistribution to both ends of the mitochondria or triggers the progressive removal of SNPH from axonal mitochondria (Figures 3A–3C). The average integrated intensity ratio of SNPH to cytochrome c on individual axonal mitochondria was not significantly reduced after 5-nM AA treatment for 2 hours (p=0.1376) and 4 hours (p=0.083). Prolonged 6-hour AA treatment is required to substantially remove SNPH from axonal mitochondria (p<0.0001) (Figure 3C); the time course correlates well with enhanced mitochondrial transport after 6 hours of AA treatment (Figures 2A, 2B). The average mitochondrial load in axons and mitochondrial size was slightly reduced after 6 hours of AA treatment (Figure 3D). Such SNPH redistribution patterns were not observed for TOM20 under the same stress conditions (Figure 3E). To further characterize SNPH vesicles, we labeled hippocampal neurons with CMTMRos followed by co-staining with SNPH and cytochrome *c* antibodies. SNPH cargo vesicles lose cytochrome *c* and $\Delta\psi_m$ (Figure 3F) and does not carry TOM20 (Figure S3), suggesting a new class of mitochondria-derived SNPH cargo vesicles.

Generation of SNPH Cargo Vesicle is Parkin- and Drp1-Independent

To characterize the nature of SNPH cargo detachment, we examined their ultra-structures by immuno-electron microscopy (Immuno-EM). We labeled endogenous SNPH with an anti-SNPH antibody in DRG neurons treated AA (5 nM) for 6 hours to induce mild mitochondrial stress. In DMSO-treated control axons, SNPH is scattered along the surface of mitochondria (Figure 4A). AA treatment triggers the budding process of SNPH in the form of cargo vesicles as their limiting membrane is continuous with the OMM (Figure 4B), which coincides with the presence of SNPH single-membrane vesicles in close proximity to mitochondria. AA treatment significantly reduces the density of SNPH-labeled gold particles on the mitochondrial surface (p<0.0001) (Figure 4C). These ultra-structural

observations provide strong evidence of the budding process of SNPH cargo vesicles from stressed mitochondria.

Given the small size of these SNPH cargo vesicles (~100 nm in diameter), we applied diffraction-unlimited stimulated emission depletion (STED) microscopy that can reach a resolution of 30–70 nm. By immunostaining endogenous SNPH and cytochrome *c* in DRG axons, we observed scattered SNPH vesicles without cytochrome c labeling along axons following mild AA treatment (Figure 4D); the density of such SNPH vesicles is relatively lower in control axons. Next, we applied time-lapse STED imaging to monitor the dynamic bulk release of GFP-SNPH from axonal mitochondria in live DRG neurons. Because expressing WT SNPH abolishes mitochondrial transport to growing tips, thus impairing neuronal growth, we chose SNPH anchoring-deficient mutant SNPH*, that reduces but not abolish mitochondrial motility. Neurons were imaged using STED microscopy at DIV3 after a 6-hour incubation with 5 nM AA. Distinct spatial localization of GFP-SNPH* and the mitochondrial matrix (DsRed-Mito) can be clearly distinguished (Figure 4E). STED time-lapse images show that GFP-SNPH* displays the same localization pattern as its endogenous SNPH (Figure 4D): either scattering along the surface of mitochondria or concentrating at ends. The expeditious release of a SNPH cargo from an axonal mitochondrion was readily observed (Figure 4E), a process occurring within only 4–8 seconds, indicating a fast pinching out of bulk SNPH in the form of cargo vesicles in response to mild mitochondrial stress.

We next examined whether the generation of SNPH cargo vesicles is dependent on Parkin. Deleting *parkin* does not change the generation and density of SNPH cargo vesicles along axons under DMSO control (p=0.56) or AA stress conditions (p=0.14) (Figures 4F, 4G), indicating a Parkin-independent generation of SNPH cargo vesicles. We further examined whether autophagy induction is associated with SNPH cargo generation. DRG neurons were co-transfected with GFP-SNPH* and mCherry-LC3 at DIV0 and treated with DMSO or 5 nM AA for 6 hours or incubated with serum-free medium (starvation) at DIV3. While starvation efficiently induces the formation of autophagic vacuoles (AVs) labeled by lipidated LC3-II (Figure S4A), autophagy is not induced following the mild mitochondrial stress. In contrast, such a mild stress triggers the generation of SNPH cargo vesicles in the absence of autophagy induction along the same axons (Figure S4B). In addition, we examined whether the generation of SNPH vesicles is through a Drp1-mediated mitochondrial fission process. DRG neurons were transfected with a dominant-negative Drp1 K38A mutant at DIV0 and treated with DMSO or AA (5 nM for 6 hours) at DIV3. The generation of SNPH cargo vesicles under both DMSO (p=0.12) and AA stress conditions (p=0.50) is not affected by expressing Drp1 K38A (Figures 4H, 4I). Our study suggests that the budding process of SNPH cargo vesicles is through a mechanism independent of Drp1-mediated mitochondrial fission.

SNPH Vesicles Share the Ride with Late Endosomes for Retrograde Transport

Next, we performed live imaging to examine whether mitochondria-derived SNPH cargos are motile along axons. While axonal mitochondrial motility is reduced upon over-expression of GFP-SNPH*, the majority (74. 34 ± 5.33%) of SNPH cargo vesicles (arrows)

budding from stationary mitochondria undergo retrograde transport along axons toward the soma (Figures 5A, 5B). Only a small portion (24.04 ± 5.03%) of SNPH cargo vesicles maintain stationary and far less (2.13 ± 1.22%) move in an anterograde direction. This motility pattern shares similarity with that of late endosomes (LEs) in axons (Cai et al., 2010; Cheng et al., 2015; Xie et al., 2015).

Given the fact that mature lysosomes are enriched in the cell body, we hypothesize that mitochondria-derived SNPH cargo vesicles are likely transported to the cell body for degradation via the endo-lysosomal pathway. We tested our hypothesis by treating DRG neurons with AA in the presence or absence of lysosomal inhibitors (LIs). Inhibiting lysosomal activity significantly increases the density of SNPH cargo vesicles along axons under mild mitochondrial stress (Figures 5C, 5D), suggesting a reduced turnover of SNPH cargo vesicles. The increased density of SNPH cargo vesicles in axons may be contributed by impaired LE transport in the presence of LIs (Lee et al., 2011). To test this possibility, we examined the relative motility of LEs in the presence or absence of AA or LIs. While AA treatment does not affect the motility of LEs, applying LIs significantly reduces the transport of LEs along axons at both directions ($p<0.0001$) (Figures 5E, 5F). We further confirmed the imaging data with biochemical assays. Mature neurons at DIV10 were treated with 5 nM AA for 6 hours in the presence or absence of lysosome or proteasome inhibitors. AA-induced SNPH degradation is abolished by LIs, but not by proteasome inhibitors (Figures 5G, 5H), thus supporting our notion of the lysosome-dependent degradation of SNPH cargo vesicles.

The motility pattern of SNPH cargo vesicles shares similarities with that of LEs in axons, raising a question as to whether SNPH vesicles ride on LEs for retrograde transport toward the soma. To address this question, we co-expressed GFP-SNPH* with mRFP-Rab7, a LE marker, in DRG neurons. When a Rab7-labeled LE passes by a stationary mitochondrion, it carries a newly generated SNPH cargo vesicle and then co-transport all the way in the retrograde direction toward the soma (Figures 6A, 6B). All of these events occur within a short time frame (84 seconds). Furthermore, both LEs and SNPH-loaded LEs share a similar retrograde velocity (LE: 0.484 ± 0.040 μm/sec, n=30; SNPH-loaded LE: 0.441 ± 0.060 μm/sec, n=30; $p=0.54$) along the same axons. Consistently, Z-stack images visualized by STED microscopy shows co-localization of Rab7 and SNPH (Figure 6C). A surface 3D reconstitution of Z-stack images reveals this vesicular SNPH structure being wrapped by a Rab7-labeled LE (Movie S5).

To further confirm that SNPH cargo vesicles ride on LE for retrograde transport, we thought to use a LE-loaded dynein adaptor Snapin that links the motor to LEs (Cai et al., 2010; Cheng et al., 2015). Disrupting dynein-Snapin coupling impairs the retrograde transport of LEs, thus providing us with a molecular tool to investigate the impact of LE transport on the removal of SNPH cargo vesicles from distal axons. We immobilized LEs in DRG neurons by expressing Snapin-L99K, a dominant-negative mutant defective in dynein-binding (Cai et al., 2010). Immobilizing LEs leads to an increased density of SNPH cargo vesicles in distal axons (Figures 6D, 6E), indicating an additive role of Snapin-L99K mutant in arresting SNPH cargo vesicles following AA treatment. Expressing Snapin-L99K selectively impairs LE retrograde transport along axons (Figure 6F), consistent with previous studies in

hippocampal, motor, and DRG neurons (Cai et al., 2010; Xie et al., 2015; Cheng et al., 2015). Taken together, our studies support a model: mitochondria-derived SNPH cargo vesicles undergo retrograde transport by riding on LEs toward the soma, where mature lysosomes are relatively enriched. These results highlight the critical role of LE retrograde transport in the turnover of SNPH cargo vesicles.

Both GFP-SNPH and GFP-SNPH* cargo vesicles share the similar retrograde velocity (Figures S5A, S5B). Expressing GFP-LC8, a dynein light chain, does not affect the density of SNPH cargo vesicles under control (p=0.35) or AA treatment conditions (p=0.75), consistent with the fact that LC8 interacts with SNPH independent of dynein complexes (Chen et al., 2009).

SNPH Pathway is Robustly Activated in the Early Stages of ALS and AD

One pathological hallmark in ALS and AD is the progressive accumulation of damaged mitochondria in distal axons (Vande Velde et al., 2011; Xie et al., 2015; Wong et al., 1995). Proper removal of dysfunctional mitochondria from axons may serve as an early protective mechanism before Parkin-mediated mitophagy is activated. However, expression of mitochondrial anchoring protein SNPH is increased in mature neurons, thus restricting the early removal of dysfunctional mitochondria from distal axons. We hypothesize that the selective release of SNPH from stressed mitochondria would enhance their transport to somatic regions for turnover or recovery in diseased neurons.

We first asked whether the bulk release of SNPH in the form of cargo vesicles is enhanced during the early asymptomatic stages of fALS-related hSOD1^{G93A} mice by examining ventral root axon bundles from P40 WT and hSOD1^{G93A} littermates. SNPH cargo vesicles are robustly increased along motor neuron axons in hSOD1^{G93A} mice relative to age-matched WT mice (p<0.0001) (Figures 7A, 7B). We further confirmed these observations at the ultrastructural levels. SNPH cargo vesicles labeled with anti-SNPH-conjugated nanogold were readily detected in the ventral root axons of hSOD1^{G93A} mice (P40); some of SNPH vesicles were budding off from mitochondria (Figure 7C). As a control, anti-SNPH-conjugated nanogold mainly labels the surface of axonal mitochondria in age-matched WT mice. Both light and EM images consistently indicate a robust activation of SNPH pathway at the early stages of fALS-linked motor neuron axons. Surprisingly, progressive mitochondrial damage depletes SNPH after disease onset at P120, while in WT mice SNPH shows no decline with age (Figures 7D, 7E). SNPH depletion is specific as no significant decline was found in other mitochondrial proteins TOM20 and PDH, and neuronal marker βIII-tubulin during the same disease progression of hSOD1^{G93A} mice (Figures S6A, S6B). Miro1 is reduced in one of three hSOD1^{G93A} mice starting at the disease onset (P120). SNPH depletion correlates with an accumulation of mitochondrial pathology in axons and rapid disease progression in the hSOD1^{G93A} mouse strain. Given what is known about hSOD1^{G93A}-dynein interactions (Zhang et al., 2007) and the reduction of the motor adaptor Miro1 in hSOD1^{G93A} motor neurons (Zhang et al., 2015), it is likely that defective motor/adaptor machineries impair the removal of damaged mitochondria from axons even though the anchoring protein SNPH is depleted in the late disease stages.

We next examined whether the SNPH-mediated response is also activated in the axons of AD-related cortical neurons cultured from mutant hAPP Tg (J20) mouse brains (Mucke et al., 2000). The density of SNPH cargo vesicles in AD axons is robustly increased ($p<0.001$) (Figures 8A, 8B). The average density of SNPH cargo vesicles is relatively higher in AD axons (15 vesicles per 100 μm) when compared with WT neurons treated with 5 nM AA for 6 hours (9–12 vesicles per 100 μm) (Figures 4G, 4I, 5D). It is likely a cumulative effect of chronic pathological stress. We further quantified the percentage of mutant hAPP neurons with detectable SNPH vesicles in axons: a gradual increase in hAPP neurons showing SNPH cargo vesicles from DIV15 (22.80% ± 2.25%) to DIV21 (42.70% ± 2.03%, $p<0.0001$), while this increase was not observed in WT neurons. These data suggest that AD-associated pathological stress induces the progressive removal of SNPH from axonal mitochondria (Figure 8C).

We also examined the relative motility of axonal mitochondria with reduced $\Delta\psi_m$ in mutant hAPP cortical neurons. Chronically stressed axonal mitochondria display reduced anterograde ($p<0.001$) and enhanced retrograde ($p=0.002$) transport when compared to same-age WT neurons (Figure 8D). These data are consistent with the biased bi-directional motility of axonal mitochondria in WT neurons in response to mild AA treatment: depolarized axonal mitochondria display reduced anterograde and enhanced retrograde transport (Figure 1F). In addition, we examined total brain SNPH levels. SNPH is largely abolished in the brains of mutant hAPP Tg mice relative to their WT littermates ($p=0.004$) (Figure 8E). As a control, there is no detectable change in the levels of other mitochondrial proteins, including TOM20, VDAC, or SOD2, in the same mutant hAPP mouse brains. Consistently, a robust reduction of SNPH levels was also detected in postmortem brain specimens from human AD patients relative to age-matched control subjects ($p<0.001$) (Figure 8F). Altogether, our study highlights that the generation of SNPH cargo vesicles ensures a quick response of axonal mitochondria to pathological stresses: dysfunctional mitochondria that are anchored in distal axons of mature neurons could be remobilized and transported back to the soma, thus maintaining mitochondrial integrity in distal axons long before mitophagy is activated. It is conceivably that the progressive mitochondrial stress would deplete SNPH, or SNPH-mediated regulation is compromised by global mitochondrial pathology. Thus, Pink/Parkin pathway would instead play a more critical role in the degradation of damaged mitochondria via mitophagy in the late disease stages of ALS and AD.

DISCUSSION

Chronic mitochondrial stress and impaired mitochondrial transport have been implicated in several major neurodegenerative diseases. Such long-term cumulative stress leads to aggregation of damaged mitochondria in distal axons. Whereas the removal of defective mitochondria from axons constitutes an early step in the maintenance of mitochondrial integrity, the underlying mechanisms remain unknown. Thus, it is critical to understand how neurons sense and remove those stressed mitochondria under physiological and pathological conditions.

SNPH-Mediated Response Removes Stressed Mitochondria from Axons

To recapitulate the chronic mitochondrial dysfunction that is associated with major neurodegenerative diseases, we applied a mild mitochondrial stress by using 5 nM AA, a 1000-times lower dosage than reported (Ashrafi et al., 2014). This AA treatment induces a mild and reversible mitochondrial stress. Axonal mitochondria respond to this stress by the selective regulation of their transport in favor of removing stressed mitochondria out of axons. This regulation is triggered by the bulk release of mitochondrial anchoring protein SNPH in the form of cargo vesicles from stressed mitochondria. Such a dynamic response is captured at ultra-structural levels (immuno-EM) and time-lapse super-resolution imaging (STED). Upon release, these SNPH cargo vesicles undergo retrograde transport en route to the endosome-lysosome pathway toward the soma for degradation. Importantly, the generation of SNPH cargo vesicles was also observed in spinal ventral root motor neuron axons during the early asymptomatic stages of fALS-related mice and in the axons of AD-related cortical neurons from mutant hAPP Tg mice. Thus, in addition to its role as an anchor for axonal mitochondria (Kang et al., 2008), our study reveals a new role of SNPH pathway in remobilizing stressed mitochondria. The bulk release of SNPH from stressed mitochondria ensures that those anchored mitochondria can be removed from axons, thus maintaining axonal mitochondrial integrity in response to various physiological and pathological stresses before triggering Parkin-mediated mitophagy and the degradation of the damaged organelles.

Relative enrichment of SNPH on axonal mitochondria determines their motile versus stationary status (Kang et al., 2008). Using optogenetically-controlled recruitment of motors and SNPH to axonal mitochondria, van Bergeijk et al (2015) further demonstrate that the relative recruitment of motors or SNPH impacts mitochondrial motility. Thus, the bulk release of SNPH shifts stressed mitochondria from the SNPH-anchored status to the motor-driven transport, thus remobilizing stressed mitochondria in distal axons. Such a response is particularly relevant to mature neurons where SNPH expression is progressively increased. To our surprise, the robust generation of SNPH cargo vesicles over disease progression leads to the depletion of SNPH in the late disease stages. In spite of SNPH depletion, aberrant aggregation of damaged mitochondria in distal axons is the one pathological hallmark of late stage ALS and AD. This may be attributed to the fact that the SNPH-mediated response can no longer rescue mitochondrial pathology as disease progresses into the later stage. Alternatively, mutant $hSOD1^{G93A}$ impairs retrograde transport by binding to dynein motors (Xie et al., 2015; Zhang et al., 2007) and amyloid β oligomers block mitochondrial transport during AD pathogenesis (Calkins et al., 2011; Decker et al., 2010; Rui and Zheng, 2016; Vossel et al., 2010). In addition, reduced mitochondrial motor adaptor Miro1 was also found in an ALS mouse model (Zhang et al., 2015). Our study further confirms the reduced Miro1 levels in one of three $hSOD1^{G93A}$ mice starting at P120. These defective motor/adaptor machineries likely impair the removal of damaged mitochondria from axons in the late disease stages even though SNPH is depleted.

The functional connection between mitochondrial transport directionality and integrity under physiological and pathological conditions remains largely unresolved. Specifically, the mechanisms coordinating the biased bi-directional transport of stressed mitochondria have

not been elucidated. Miller and Sheetz (2004) reported that in DRG neurons ~80% of mitochondria with reduced $\Delta\psi_m$ was transported toward the soma. Using the same neurons, Verburg and Hollenbeck (2008) showed no difference in the $\Delta\psi_m$ between mobile and stationary mitochondria under non-stress conditions. In the current study, ~80% of depolarized mitochondria undergo retrograde transport following the release of SNPH cargo vesicles under mild stress conditions (Figure 1F). Consistently, depolarized axonal mitochondria in mutant hAPP cortical neurons also display reduced anterograde and enhanced retrograde transport when compared to same age WT neurons (Figure 8D). Thus, under mild stress and chronic pathological conditions, releasing SNPH from dysfunctional mitochondria constitutes a key early step in enhancing their retrograde transport.

SNPH Mediates An Early Response Before Parkin-Mediated Mitopahgy Is Activated

The generation of SNPH cargo vesicles from stressed axonal mitochondria is initiated as early as 6 hours of mild stress conditions. In contrast, Parkin-mediated mitophagy is not readily detected until 30 hours under the same stress conditions (Figure S1). In addition, *parkin* KO neurons display no impaired generation of SNPH cargo vesicles when compared with WT neurons (Figures 4F. 4G). Thus, we propose that the SNPH-mediated stress response is critical to maintaining axonal mitochondrial integrity long before Parkin-mediated mitophagy is activated. When mitochondria undergo acute and global damaged, this early mechanism is likely bypassed or compromised by activating mitophagy to eliminate dysfunctional organelles (Ashrafi et al., 2014). The broad time window left in the pre-mitophagy phase in cultured neurons and in the pre-symptomatic stages of disease models suggest that the SNPH-mediated pathway is an early mechanism for axonal mitochondrial quality control.

Our previous study revealed that Parkin-mediated mitophagy mainly occurs in the somatodendritic regions of mature cortical neurons (Cai et al., 2012). Axonal mitophagy is induced by an acute treatment of neurons with a high dosage of AA (40 μM) (Ashrafi et al., 2014), a condition likely exceeds the physiological limits that activate SNPH pathway. Indeed, acute mitochondrial depolarization in neurons suddenly arrests mitochondrial transport by PINK1/Parkin-mediated Miro1 degradation (Wang et al., 2011) and quickly induces mitochondrial fragmentation (Ashrafi et al., 2014). If the acute depolarization model operates *in vivo*, one would expect the accumulation of damaged mitochondria in distal axons following genetic mutation of the PINK1-Parkin pathway that results in mitophagy failure. This model has recently been re-examined by an *in vivo* study. Mutation of Parkin in *Drosophila* does not accumulate damaged mitochondria in motor neuron axons or neuromuscular junctions; instead it impairs the mitochondrial turnover that is mainly restricted to the soma in the intact nervous system (Sung et al., 2016). Thus, under chronic mitochondrial stress or pathological conditions, early removal of those dysfunctional mitochondria from axons constitutes an important pathway to maintain axonal mitochondrial integrity. In mature neurons, a majority of mitochondria distribute separately along distal axons and in synaptic terminals. It is conceivable that stressed mitochondria anchored in distal axons will largely limit their quality control mechanisms through fusion/fission events or dynamic ER-mitochondrial contacts. Enhanced the motility of stressed mitochondria

facilitates their membrane dynamics and contacts with ER, thus likely increasing their recovery.

SNPH Cargo Is A New Class of Axonal Mitochondria-Derived Vesicles

In many non-neuronal cell types, the entire mitochondrial network can be quickly degraded through mitophagy under certain acute stress conditions (Geisler et al., 2010; Narendra et al., 2008). Since the ATP source in neurons mainly comes from mitochondria, neurons instead possess an early protective mechanism to maintain mitochondrial integrity in distal axons under mild stress conditions. Recent studies suggest that the generation of mitochondrial-derived vesicles (MDVs) in non-neuronal cells can efficiently remove damaged or aggregated protein in order to avoid the complete degradation of whole organelles (Sugiura et al., 2014). The criterion to define a MDV is evidence of cargo selectivity (Neuspiel et al., 2008). The generation of MDVs does not require the activation of autophagy machinery as it occurs in the absence of the key autophagic components Atg5, Rab9, or beclin1 (Soubannier et al, 2012; McLelland et al, 2014). In non-neuronal cells, MDVs are generated through the selective incorporation of mitochondrial protein cargoes independent of the GTPase Drp1 (Neuspiel et al., 2008). Two subsets of MDVs have been characterized based on their trafficking destination: either targeted to peroxisomes (Neuspiel et al., 2008) or transported to LE/lysosomal system (Soubannier et al., 2012). It has been thought that the selective incorporation of different protein cargoes depends on the nature of the mitochondrial stress. In Hela and COS7 cells under oxidative stress, cargo-selective MDVs include (1) $TOM20^{+}/Matrix^{-}$ MDVs containing the OMM protein TOM20 and (2) $TOM20^{-}/Matrix^{+}$ MDVs containing the mitochondrial matrix proteins.

Our study reveals a new class of axonal mitochondria-derived selective cargos that release bulk SNPH under physiological paradigms in axonal compartments, where mitochondrial trafficking and anchoring are unique from non-neuronal cell types. By using immuno-EM and time-lapse super-resolution microscopy, we demonstrated the dynamic budding process of SNPH in the form of cargos from stressed axonal mitochondria and the transport of these cargos en route to LEs/lysosomes for degradation. To our knowledge, this is the first observation showing the mitochondria-derived organelles in axons under physiological and pathological stress conditions. Axonal SNPH cargos and non-neuronal $TOM20^{+}/Matrix^{-}$ MDVs share some common features: (1) the formation of both vesicles is LC3-, Parkin- and Drp1-independent; (2) both vesicles form from the lateral segregation of the mitochondrial membrane; and (3) both vesicles are delivered to LEs/lysosomes for degradation. However, our study also reveals several unique features of SNPH cargo vesicles. First, the generation of SNPH cargo vesicles is mainly found in axonal mitochondria. Second, SNPH cargo vesicles are generated at an earlier time point under mild stress conditions in neurons long before Parkin-mediated mitophagy is activated. While SNPH vesicles can be frequently observed in axons as early as 6 hours after the treatment with 5 nM AA, $TOM20^{+}$ MDVs were hardly detectable in axons at the same stages (Figure 3E). Third, while MDVs maintain detectable $\Delta\psi_m$ as seen by the loading of TMRE (Soubannier et al., 2012), SNPH cargo vesicles lose cytochrome *c* and $\Delta\psi_m$ (Figure 3F) and does not carry TOM20 (Figure S3). Fourth, SNPH is an axonal mitochondrial docking protein. The selective bulk removal of SNPH from stressed mitochondria remobilizes those mitochondria in response to early stress

conditions. Taken together, the generation of SNPH cargo vesicles is a unique neuronal mechanism that enables the fine coordination of mitochondrial motility and integrity. It is likely the first-line mitochondrial defense that sits in the early stage of the complete hierarchy of the mitochondrial quality control system in axons. Thus, our study reveals a new neuronal pathway that benefits the development of strategies to attenuate axonal mitochondrial pathology in the early stages of several major neurodegenerative diseases.

STAR * METHODS

CONTACT FOR REAGENT AND RESOURCE SHARING

Further information and requests for resources and reagents should be directed to and will be fulfilled by the Lead Contact, Zu-Hang Sheng (shengz@ninds.nih.gov).

EXPERIMENTAL MODEL AND SUBJECT DETAILS

Mouse lines and animal care—The *snph*$^{-/-}$ mouse line was generated as previously described (Kang et al., 2008). The hSOD1^{G93A} mice (the B6.Cg-Tg (SOD1^{G93A})1Gur/J), *parkin*$^{-/-}$ mice (B6.129S4-Park2tm1Shn/J), and mutant hAPP mice from line J20 (B6.Cg-Tg(PDGFB-APPSwInd) (Mucke et al., 2000) were purchased from the Jackson Laboratory. For preparing *snph*$^{-/-}$ neuronal cultures, four pairs of WT and *snph* KO E18 embryonic mice (sex: random) were used in four independent experiments. For ALS-related moue studies, three pairs of male WT and SOD1^{G93A} littermate at P40 were used for immunofluorescence staining and immuno-EM study, respectively. At least three pairs of male WT and SOD1^{G93A} littermate at each age group (P40, P80, P120, and P150) were used for western blot analysis. For AD-related study, three pairs of female WT and mutant hAPP littermates at 7–9 months of age were used. All mouse lines were maintained in C57BL/6J background for at least ten generations. The mice and the Sprague-Dawley rats were maintained in the NINDS animal facility and housed in a 12-hour light/dark cycle. All animal procedures were carried out following NIH guidelines and were approved by the NINDS/NIDCD Animal Care and Use Committee and the Rutgers Institutional Animal Care and Use Committee (IACUC). The animal facilities at Rutgers University are fully AAALAC accredited.

Human brain specimens—Postmortem brain specimens from AD patients and age-matched control subjects were obtained from the Harvard Tissue Resource Center and the Human Brain and Spinal Fluid Resource Center at UCLA. Specimens were from patients diagnosed with AD according to Braak criteria (Braak and Braak, 1991). The specimens were from the frontal cortex and were quick-frozen (BA9). Three control subjects and nine patient brains in different Braak stages with postmortem interval 7.08 hr – 22.5 hr were used for analysis.

Case type	Age/sex	Postmortem interval (h)	Braak stage of AD brains
Control #1	75/F	20.1	0
Control #2	87/M	9.3	0

Case type	Age/sex	Postmortem interval (h)	Braak stage of AD brains
Control #3	47/M	12.5	0
AD #1	65/M	18.6	Braak I
AD #2	82/F	15.7	Braak I
AD #3	72/M	21.8	Braak II
AD #4	86/M	9.00	Braak III
AD #5	86/M	17.4	Braak III
AD #6	60/F	15.2	Braak V
AD #7	78/M	20.87	Braak V
AD #8	66/M	10.5	Braak VI
AD #9	86/F	7.08	Braak VI

Primary neuron cultures—Hippocampal and cortical neurons were collected from E18 embryonic rats or mice (sex: random) as previously described (Kang et al., 2008). After dissociation by papain, neurons were re-suspended in the plating medium (for 10 ml of plating medium: 9 ml Neurobasal medium [Invitrogen], 0.5 mM Glutamax, 0.25 mg insulin, 10% fetal bovine serum, 2% B-27 medium supplement, 0.1% 2-Mercaptoenthanol) and plated onto 12-mm coverslips coated with poly-orthinine (Sigma-Aldrich; 1:4 in PBS) and laminin (Roche; diluted 1:500 in PBS). After 24 hours of growing neurons in plating medium, half of the plating medium was replaced with the same amount of neuronal feeding medium (2% B27 and 0.5 mM Glutamax in Neurobasal medium). Cells were fed every three days by aspirating half the medium and replacing it with the same amount of neuronal feeding medium. Neurons were transfected with various constructs at DIV6 by using the calcium phosphate method, and imaged at DIV9–10 with confocal microscopy.

DRG neurons were isolated from post-natal 8–10 days (P8–P10) Sprague-Dawley rat (sex: random) spinal cord or male P90 mouse spinal cord in Hank's buffered salt solution and digested in 2.5 units/ml dispase II (Roche Applied Science) and 200 units/ml collagenase (Worthington Biochemical) at 37°C for 30 min followed by a 35-min shaking at room temperature. Neurons were then collected with a 70 μm nylon cell strainer (Falcon). Before plating, DRG neurons were transfected with various plasmid DNA. We used a Nucleofector (Lonza) for transfection according to the manufacturer's specifications and plated on coverslips coated with poly-ornithine (Sigma; diluted 1:3 in ddH20) and laminin (Roche; diluted 1:500 in PBS). Neurons were then maintained in Neurobasal-A medium supplemented with 2.5% fetal bovine serum, 0.5 mM Glutamax, and B27 (Invitrogen) for 2–3 days at 37 °C in a 5% CO_2 incubator.

METHOD DETAILS

DNA constructs—mRFP-Rab7 was purchased from Addgene. GFP-SNPH* (Chen and Sheng, 2013) and lentivirus-expressed HA-SNPH, HA-Miro1 and GFP-Mito (Zhou et al., 2016) were generated previously. The GFP-Parkin plasmid was constructed by replacing YFP in the YFP-Parkin plasmid with EGFP. Full length Parkin was amplified by PCR using a 5′ primer containing the NheI site 5′-CGTCAGATCC GCTAGCGCTA and the 3′ primer containing the BsrGI site 5′-ACTTGTACAG CTCGTCCATG. DsRed-Mito, GFP-Mito, and

mcherry-LC3 are gifts from Dr. R. Youle (NINDS, NIH, MD). These constructs were verified by DNA sequencing.

Live neuron imaging analysis—For hippocampal and cortical neurons, proximal axonal segments were selected for live imaging along single processes distinct from others in the field—segments with crossing or fasciculation were excluded from analysis. Axon can be recognized by their unique morphological characteristics: long, thin, and uniform in diameter with growth cones and sparse branches (Banker and Cowan, 1977). Axonal mitochondria are small and vesicular in structure, and are sparsely distributed throughout the axon; in contrast, dendritic mitochondria are elongated or filamentous and occupy a large proportion of the neurite (Chang et al., 2006; Popov et al., 2005). Transfected neurons were transferred to Tyrode's buffer (10 mM Hepes, 10 mM glucose, 1.2 mM $CaCl_2$, 1.2 mM $MgCl_2$, 3 mM KCl and 145 mM NaCl, pH 7.4) and imaged at 37°C under an air stream incubator. Cells were imaged with a 40x 1.3 NA oil immersion objective on a LSM 510 or 880 Zeiss confocal microscope. Time-lapse images were acquired at a 512 × 512 pixel resolution. Kymographs were generated by ImageJ (NIH) and converted to QuickTime video. If a mitochondrion remained immotile for the entire recording period, it is classified as stationary. In contrast, only if the displacement ≥10 μm would be considered as motile. SNPH-positive and Cyto C-negative vesicles were identified by eye and quantified in three independent experiments.

For DRG neurons, imaging was performed in Low Fluorescence Hibernate A media (BrainBits) with 0.5 mM Glutamax and B27. Neurons were time-lapse imaged under an environmental chamber where temperature was maintained at 37°C and CO_2 concentration at 5%. DRG neurons were visualized with a Zeiss LSM 880 oil immersion 63x objective. Kymographs were generated by ImageJ (NIH) and converted to QuickTime movies. A motile mitochondrion in either direction was counted only if the net displacement (total plus versus minus distance) was ≥ 10 μm. The number of SNPH vesicles were identified by eye and quantified in three independent experiments.

The durations and intervals for time-lapse imaging depend on (1) the nature of the organelles, (2) photo-stability of the fluorophore under laser scanning, (3) cultured chambers used, and (4) single versus dual-channel time-lapse imaging. For recording late endosomes (LE) and LE-carried vesicles that are of fast moving organelles, 2-second intervals with a 3-minute short recording time is sufficient to catch their trajectory, whereas for recording mitochondria, 5-second intervals with an 8–10-min recording is a proper duration to show their relative motility along axons. For recording mitochondrial flux passing through microgrooves in microfluidic chambers, relative mitochondrial flux events along axonal bundles were captured for a total of 100 frames with 5-second intervals for 10 minutes. For dual-channel time-lapse imaging of both SNPH vesicles and late endosomes along axons, images were taken consecutively every 2-second with green channel followed by the red channel for total duration of 3 minutes.

Super-resolution STED imaging—The inverted STED microscope with resolution of ~50–90 nm (TCS SP8 STED 3X, Leica, Germany) was used. For fixed-cell imaging, GFP/Atto 488 were excited by a tunable white light laser (70% of maximum power) at 470 nm

(10%) with the STED depletion laser at 592 nm (25% of the maximum power); its fluorescence at 480–560 nm was collected using time-gated detection (1.5–6.5 ns). mRFP/Alexa Fluor 594 were excited by the tunable white light laser at 558 nm/594 nm (10%) with the STED depletion laser at 660 nm (60% of the maximum power); its fluorescence between 575–650/600–650 nm was collected using time-gated detection (0.5–6.5 ns). For dual-color imaging of mRFP/Alexa Fluror 594 and GFP/Atto 488, mRFP/Alexa Fluror 594 was first imaged to avoid bleaching by the 592nm STED depletion laser with a frame-scanning mode. For live-cell imaging, GFP was excited by a tunable white light laser (70% of maximum power) at 470 nm (10%) with the STED depletion laser at 660 nm (60% of the maximum power); its fluorescence at 480–530 nm was collected using time-gated detection (1.5–6.5 ns). DsRed was excited by the tunable white light laser at 558 nm (10%) with the STED depletion laser at 660 nm (60% of the maximum power); its fluorescence between 575–650nm was collected using time-gated detection (0.5–6.5 ns). Images were continuously captured with 4.17 seconds between each frame (the average of 16 times) using a resonant scanner. DsRed was imaged first followed by GFP with a line-scanning mode. Z-stack images were taken consecutively with 110 nm between each step. Images were subject to deconvolution processing followed by maximum projection or 3D reconstitution using Huygens software.

Immuno-electron microscopy—Immuno-electron microscopy was performed using a rabbit polyclonal antibody against endogenous SNPH by applying the pre-embedding gold enhancement method. Briefly, cultured rat DRG neurons at DIV3 were fixed at room temperature with an EM fixative (0.1% glutaraldehyde with 4% paraformaldehyde in PBS) for 30 mins after DMSO or AA treatment. After 5 washes (5 min each) with PBS, neurons were blocked and permeabilized with PBS containing 5% normal goat serum and 0.1% saponin for 30 mins. The neurons were then incubated with a primary antibody made in PBS with 5% normal goat serum and 0.05% saponin for 1 hour at room temperature. The primary antibodies were removed and the neurons were washed 5 times (5 min each) with PBS. The neurons were then incubated in nanogold Fab' conjugates (1:200 dilution) (Nanoprobe) made in PBS containing 5% normal goat serum and 0.05% saponin for another hour at room temperature. The secondary antibodies were removed and the neurons were washed 5 times with PBS. The immunogold-labeled neurons were then fixed with 2% (w/v) glutaraldehyde in PBS overnight at 4°C. After washing with deionized water 5 times for 5 mins each, the gold labeling was intensified by using a silver enhancement kit (Nanoprobe) for 8.5 min in the dark. After intensified washing in distilled water followed by PBS, neurons were treated with PBS containing 0.2% OsO_4 for 30 mins, en bloc mordanted with uranyl acetate, dehydrated through a series of graded ethanol washes, and embedded in epoxy resins. Thin sections were stained with uranyl acetate and lead citrate (EM Facility, National Institute of Neurological Disorders and Stroke, National Institutes of Health). Images were acquired on a JEOL 200CX electron microscope and analyzed using ImageJ (NIH).

WT and $hSOD1^{G93A}$ littermates were anesthetized and transcardially perfused with EM fixative (0.05% glutaraldehyde with 4% paraformaldehyde in PBS). Ventral root axons were isolated quickly and were put in the same EM fixative within 30 minutes after perfusion.

After 5 washes (5 min each) with PBS, samples were processed for immune-gold staining as described above.

Western blot—Cortical neurons at DIV10 were treated with DMSO or 5 nM Antimycin A in the presence or absence of a lysosome inhibitor or proteasome inhibitor at different time points. Cell were collected and lysed with RIPA buffer (50 mM Tris-HCl, pH 7.5, 150 mM NaCl, 1% Triton X-100, 0.1% SDS, 0.5 % DOC) with protease inhibitors. Equal amounts of proteins were loaded and analyzed by 4–12% Bris-Tris NuPAGE and Western blot.

Measurement of mitochondria $\Delta\psi_m$—Hippocampal neurons were transfected with GFP-Mito at DIV 6 and at DIV10 were treated with DMSO or 5 nM AA for 6 hours followed by loading with 10 nM MitoTracker Green and 25 nM of the mitochondrial membrane potential-dependent dye TMRE for 20 minutes before imaging. For the microfluidic chamber, GFP-Mito was introduced into cultured neurons to label total mitochondria at DIV0. At DIV8, 5 nM AA was applied to the axonal chamber for 3 or 6 hours and then washed out with fresh medium. Right after 5 nM AA treatment or recovery for 1 hour, 100 nM MitoTracker CMTMRos, a fixable $\Delta\psi_m$-dependent dye, was loaded in the axonal chamber for 20 minutes, then washed three times with PBS and fixed for imaging. $\Delta\psi_m$ was assessed by the relative MitoTracker CMTMRos fluorescence intensity of each individual mitochondrion labeled by GFP-Mito in the axonal chamber using ImageJ particle analysis.

Microfluidic chamber preparation—A silicon wafer with a pattern made out of SU-8 by photolithography was used to cast the house-made PDMS microfluidic devices. Briefly, the SYLGARD 184 SILICONE elastomer base was mixed with the curing agent at a ratio of 10:1. The PDMS was then mixed well using a THINKY mixer ARF-310 in two steps: mixing at 2000 rpm for 4 min and de-foaming at 2200 rpm for 4 min. The well-mixed PDMS was poured onto the silicon wafer and then placed in a Bel-Art vacuum desiccator for 3 hours to help remove air bubbles from the PDMS. The wafer with PDMS was placed in an 80°C oven for 1 hour to cure. Once the PDMS was cured, the PDMS was pulled out, and reservoirs were punched out. The PDMS devices were extensively washed and autoclaved before use.

Lentivirus production and infection—HEK293T cells were transfected with the vector, psPAX2, and pMD2G at a 4:2:1 ratio to produce the lentivirus. After a 24-hour transfection, the medium was aspirated and replaced with 7 ml of UltraCulture™ medium. Virus-containing media were collected after a 48hr and 72hr transfection and then centrifuged at 1500 rpm for 5 minutes to remove cell debris. The pre-cleaned supernatant was collected and ultra-centrifuged at 90,000 g for 1.5 hours. The supernatant was carefully removed and PBS was added to resuspend the viral pellets. The concentrated virus was aliquoted and stored at −80°C until use. 2×10^5 of freshly dissociated cortical neurons were infected with a concentrated lentivirus containing GFP-Mito and HA, HA-SNPH or HA-Miro1 in 25 μl culture medium for 10 minutes and then added to the cell body chamber of the microfluidic chamber. 100 μl of culture media were added to each well of the device after 20 minutes.

Immunofluorescence—Cells were fixed with PBS containing 4% formaldehyde and 4% sucrose for 15 min at room temperature and washed with PBS three times. After permeabilization with 0.1% Triton X-100 in PBS for 15 min, cells were blocked with PBS containing 1% BSA and 5% goat serum for 1 h. Various primary antibodies diluted in blocking buffer were added to the cells and incubated at 4°C overnight. Cells were washed with PBS three times and labeled with a fluorescence-conjugated secondary antibody. After washing with PBS three times, neurons were mounted with anti-fade mounting medium (Fluoro-Gel; Electron Microscopy Sciences) for imaging.

Mice were anesthetized and transcardially perfused sequentially with 1x PBS and 4% paraformaldehyde in PBS. Tissues were removed followed by post-fixation in 4% paraformaldehyde overnight and soaked in 30% sucrose. Axon sections (3–5 μm thick) were obtained with a Leica CM3050S cryostat. The sections were washed in PBS and processed for immunofluorescence staining as described above.

QUANTIFICATION AND STATISTICAL ANALYSIS

All quantifications were performed not blinded. Statistical parameters including the definitions and exact value of n (e.g. number of experiments or replications, number of axons, number of organelles, number of images, number of neurons, number of slice sections, number of animals or human samples, etc), deviations, p values, and the types of the statistical tests are reported in the Figures and corresponding Figure Legends. Statistical analysis was carried out using Prism 7 (Graphpad Software). All statistical comparisons were conducted on data originating from three or more biologically independent experimental replicates. Comparisons between groups were planned before statistical testing and target effect sizes were not predetermined. Statistical comparisons between two groups were performed by an unpaired *t* test (sample size ≥30) or a Mann-Whitney test (sample size <30). Comparisons between three or more groups were performed by one-way analysis of variance (ANOVA) with post hoc testing by a Dunnett's multiple comparisons test or a Tukey's multiple comparisons test where otherwise indicated. Data are expressed as mean ± SEM. Differences were considered significant with $p<0.05$.

Supplementary Material

Refer to Web version on PubMed Central for supplementary material.

Acknowledgments

We thank members of the Sheng lab for technical assistance and constructive discussion; S. Cuddy and T. Farfel-Becker for critical reading; R. Youle (NINDS, NIH) and D. Trono (EPFL) for constructs; N. Morgan (NIBIB, NIH) for design and fabrication of microfluidic device templates; S. Cheng (NINDS EM Facility) for immuno-EM, and NINDS Light Imaging Facility, C.-C. Lin (NIDDK, NIH) for the Seahorse assays using T. Finkel's equipment (NHLBI, NIH), P. J. Wen for STED imaging. The work was supported by the Intramural Research Program of NINDS, NIH ZIA NS003029 and ZIA NS002946 (Z-H. Sheng) and NIH R01NS089737 (Q. Cai).

Abbreviations

AA	Antimycin A1
AD	Alzheimer's disease

AV	autophagic vacuole
DIV	days *in vitro*
DRG	dorsal root ganglion
fALS	familial amyotrophic lateral sclerosis
KO	knockout
LE	late endosome
MC	microgroove channels
MDVs	mitochondrial-derived vesicles
MT	microtubule
OMM	outer mitochondrial membrane
P60	postnatal day 60
SNPH	syntaphilin
SNPH*	SNPH anchoring deficient mutant
TMRE	tetramethylrhodamine ethylester
WT	wild-type
$\Delta\psi_m$	mitochondrial membrane potential

References

Ashrafi G, Schlehe JS, LaVoie MJ, Schwarz TL. Mitophagy of damaged mitochondria occurs locally in distal neuronal axons and requires PINK1 and Parkin. J Cell Biol. 2014; 206:655–670. [PubMed: 25154397]

Banker GA, Cowan WM. Further Observations on Hippocampal-Neurons in Dispersed Cell-Culture. J Comp Neurol. 1979; 187:469–493. [PubMed: 385643]

Braak H, Braak E. Neuropathological stageing of Alzheimer-related changes. Acta Neuropathol. 1991; 82:239–259. [PubMed: 1759558]

Birsa N, Norkett R, Higgs N, Lopez-Domenech G, Kittler JT. Mitochondrial trafficking in neurons and the role of the Miro family of GTPase proteins. Biochem Soc Trans. 2013; 41:1525–1531. [PubMed: 24256248]

Cai Q, Lu L, Tian JH, Zhu YB, Qiao H, Sheng ZH. Snapin-regulated late endosomal transport is critical for efficient autophagy-lysosomal function in neurons. Neuron. 2010; 68:73–86. [PubMed: 20920792]

Cai Q, Zakaria HM, Simone A, Sheng ZH. Spatial parkin translocation and degradation of damaged mitochondria via mitophagy in live cortical neurons. Curr Biol. 2012; 22:545–552. [PubMed: 22342752]

Calkins MJ, Manczak M, Mao P, Shirendeb U, Reddy PH. Impaired mitochondrial biogenesis, defective axonal transport of mitochondria, abnormal mitochondrial dynamics and synaptic degeneration in a mouse model of Alzheimer's disease. Hum Mol Genet. 2011; 20:4515–4529. [PubMed: 21873260]

Chang DT, Reynolds IJ. Mitochondrial trafficking and morphology in healthy and injured neurons. Prog Neurobiol. 2006; 80:241–268. [PubMed: 17188795]

Chen H, Chan DC. Mitochondrial dynamics--fusion, fission, movement, and mitophagy--in neurodegenerative diseases. Hum Mol Genet. 2009; 18:R169–176. [PubMed: 19808793]

Chen YM, Gerwin C, Sheng ZH. Dynein light chain LC8 regulates syntaphilin-mediated mitochondrial docking in axons. J Neurosci. 2009; 29:9429–9438. [PubMed: 19641106]

Chen Y, Sheng ZH. Kinesin-1-syntaphilin coupling mediates activity-dependent regulation of axonal mitochondrial transport. J Cell Biol. 2013; 202:351–364. [PubMed: 23857772]

Cheng XT, Zhou B, Lin MY, Cai Q, Sheng ZH. Axonal autophagosomes recruit dynein for retrograde transport through fusion with late endosomes. J Cell Biol. 2015; 209:377–386. [PubMed: 25940348]

De Vos KJ, Chapman AL, Tennant ME, Manser C, Tudor EL, Lau KF, Brownlees J, Ackerley S, Shaw PJ, McLoughlin DM, et al. Familial amyotrophic lateral sclerosis-linked SOD1 mutants perturb fast axonal transport to reduce axonal mitochondria content. Hum Mol Genet. 2007; 16:2720–2728. [PubMed: 17725983]

Decker H, Lo KY, Unger SM, Ferreira ST, Silverman MA. Amyloid-beta peptide oligomers disrupt axonal transport through an NMDA receptor-dependent mechanism that is mediated by glycogen synthase kinase 3beta in primary cultured hippocampal neurons. J Neurosci. 2010; 30:9166–9171. [PubMed: 20610750]

Devireddy S, Liu A, Lampe T, Hollenbeck PJ. The Organization of Mitochondrial Quality Control and Life Cycle in the Nervous System In Vivo in the Absence of PINK1. J Neurosci. 2015; 35:9391–9401. [PubMed: 26109662]

Ferree AW, Trudeau K, Zik E, Benador IY, Twig G, Gottlieb RA, Shirihai OS. MitoTimer probe reveals the impact of autophagy, fusion, and motility on subcellular distribution of young and old mitochondrial protein and on relative mitochondrial protein age. Autophagy. 2013; 9:1887–1896. [PubMed: 24149000]

Geisler S, Holmstrom KM, Treis A, Skujat D, Weber SS, Fiesel FC, Kahle PJ, Springer W. The PINK1/Parkin-mediated mitophagy is compromised by PD-associated mutations. Autophagy. 2010; 6:871–878. [PubMed: 20798600]

Kang JS, Tian JH, Pan PY, Zald P, Li C, Deng C, Sheng ZH. Docking of axonal mitochondria by syntaphilin controls their mobility and affects short-term facilitation. Cell. 2008; 132:137–148. [PubMed: 18191227]

Lee S, Sato Y, Nixon RA. Lysosomal proteolysis inhibition selectively disrupts axonal transport of degradative organelles and causes an Alzheimer's-like axonal dystrophy. J Neurosci. 2011; 31:7817–7830. [PubMed: 21613495]

McLelland GL, Soubannier V, Chen CX, McBride HM, Fon EA. Parkin and PINK1 function in a vesicular trafficking pathway regulating mitochondrial quality control. EMBO J. 2014; 33:282–295. [PubMed: 24446486]

Miller KE, Sheetz MP. Axonal mitochondrial transport and potential are correlated. J Cell Sci. 2004; 117:2791–2804. [PubMed: 15150321]

Mucke L, Masliah E, Yu GQ, Mallory M, Rockenstein EM, Tatsuno G, Hu K, Kholodenko D, Johnson-Wood K, McConlogue L. High-level neuronal expression of abeta 1–42 in wild-type human amyloid protein precursor transgenic mice: synaptotoxicity without plaque formation. J Neurosci. 2000; 20:4050–4058. [PubMed: 10818140]

Narendra D, Tanaka A, Suen DF, Youle RJ. Parkin is recruited selectively to impaired mitochondria and promotes their autophagy. J Cell Biol. 2008; 183:795–803. [PubMed: 19029340]

Neuspiel M, Schauss AC, Braschi E, Zunino R, Rippstein P, Rachubinski RA, Andrade-Navarro MA, McBride HM. Cargo-selected transport from the mitochondria to peroxisomes is mediated by vesicular carriers. Curr Biol. 2008; 18:102–108. [PubMed: 18207745]

Perlson E, Jeong GB, Ross JL, Dixit R, Wallace KE, Kalb RG, Holzbaur EL. A switch in retrograde signaling from survival to stress in rapid-onset neurodegeneration. J Neurosci. 2009; 29:9903–9917. [PubMed: 19657041]

Popov V, Medvedev NI, Davies HA, Stewart MG. Mitochondria form a filamentous reticular network in hippocampal dendrites but are present as discrete bodies in axons: a three-dimensional ultrastructural study. J Comp Neurol. 2005; 492:50–65. [PubMed: 16175555]

Rui Y, Zheng JQ. Amyloid beta oligomers elicit mitochondrial transport defects and fragmentation in a time-dependent and pathway-specific manner. Mol Brain. 2016; 9:79. [PubMed: 27535553]

Saxton WM, Hollenbeck PJ. The axonal transport of mitochondria. J Cell Sci. 2012; 125:2095–2104. [PubMed: 22619228]

Schon EA, Przedborski S. Mitochondria: the next (neurode)generation. Neuron. 2011; 70:1033–1053. [PubMed: 21689593]

Schwarz TL. Mitochondrial trafficking in neurons. Cold Spring Harb Perspect Biol. 2013:5.

Sheng ZH. Mitochondrial trafficking and anchoring in neurons: New insight and implications. J Cell Biol. 2014; 204:1087–1098. [PubMed: 24687278]

Sheng, ZH. The interplay of axonal energy homeostasis and mitochondrial trafficking and anchoring. Trends in Cell Biology. 2017. (http://dx.doi.org/10.1016/j.tcb.2017.01.005)

Sheng ZH, Cai Q. Mitochondrial transport in neurons: impact on synaptic homeostasis and neurodegeneration. Nat Rev Neurosci. 2012; 13:77–93. [PubMed: 22218207]

Soubannier V, McLelland GL, Zunino R, Braschi E, Rippstein P, Fon EA, McBride HM. A vesicular transport pathway shuttles cargo from mitochondria to lysosomes. Curr Biol. 2012a; 22:135–141. [PubMed: 22226745]

Sugiura A, McLelland GL, Fon EA, McBride HM. A new pathway for mitochondrial quality control: mitochondrial-derived vesicles. EMBO J. 2014; 33:2142–2156. [PubMed: 25107473]

Sung H, Tandarich LC, Nguyen K, Hollenbeck PJ. Compartmentalized Regulation of Parkin-Mediated Mitochondrial Quality Control in the Drosophila Nervous System In Vivo. J Neurosci. 2016; 36:7375–7391. [PubMed: 27413149]

van Bergeijk P, Adrian M, Hoogenraad CC, Kapitein LC. Optogenetic control of organelle transport and positioning. Nature. 2015; 518:111–114. [PubMed: 25561173]

Van Laar VS, Arnold B, Cassady SJ, Chu CT, Burton EA, Berman SB. Bioenergetics of neurons inhibit the translocation response of Parkin following rapid mitochondrial depolarization. Hum Mol Genet. 2011; 20:927–940. [PubMed: 21147754]

Vande Velde C, McDonald KK, Boukhedimi Y, McAlonis-Downes M, Lobsiger CS, Bel Hadj S, Zandona A, Julien JP, Shah SB, Cleveland DW. Misfolded SOD1 associated with motor neuron mitochondria alters mitochondrial shape and distribution prior to clinical onset. PLoS One. 2011; 6:e22031. [PubMed: 21779368]

Verburg J, Hollenbeck PJ. Mitochondrial membrane potential in axons increases with local nerve growth factor or semaphorin signaling. J Neurosci. 2008; 28:8306–8315. [PubMed: 18701693]

Vonderheit A, Helenius A. Rab7 associates with early endosomes to mediate sorting and transport of Semliki forest virus to late endosomes. PLoS Biol. 2005; 3:e233. [PubMed: 15954801]

Vossel KA, Zhang K, Brodbeck J, Daub AC, Sharma P, Finkbeiner S, Cui B, Mucke L. Tau reduction prevents Abeta-induced defects in axonal transport. Science. 2010; 330:198. [PubMed: 20829454]

Wang X, Winter D, Ashrafi G, Schlehe J, Wong YL, Selkoe D, Rice S, Steen J, LaVoie MJ, Schwarz TL. PINK1 and Parkin target Miro for phosphorylation and degradation to arrest mitochondrial motility. Cell. 2011; 147:893–906. [PubMed: 22078885]

Wong PC, Pardo CA, Borchelt DR, Lee MK, Copeland NG, Jenkins NA, Sisodia SS, Cleveland DW, Price DL. An adverse property of a familial ALS-linked SOD1 mutation causes motor neuron disease characterized by vacuolar degeneration of mitochondria. Neuron. 1995; 14:1105–1116. [PubMed: 7605627]

Xie Y, Zhou B, Lin MY, Wang S, Foust KD, Sheng ZH. Endolysosomal Deficits Augment Mitochondria Pathology in Spinal Motor Neurons of Asymptomatic fALS Mice. Neuron. 2015; 87:355–370. [PubMed: 26182418]

Zhang F, Wang W, Siedlak SL, Liu Y, Liu J, Jiang K, Perry G, Zhu X, Wang X. Miro1 deficiency in amyotrophic lateral sclerosis. Front Aging Neurosci. 2015; 7:100. [PubMed: 26074815]

Zhang FJ, Strom AL, Fukada K, Lee S, Hayward LJ, Zhu HN. Interaction between familial amyotrophic lateral sclerosis (ALS)-linked SOD1 mutants and the dynein complex. J Biol Chem. 2007; 282:16691–16699. [PubMed: 17403682]

Zhou B, Yu P, Lin MY, Sun T, Chen Y, Sheng ZH. Facilitation of axon regeneration by enhancing mitochondrial transport and rescuing energy deficits. J Cell Biol. 2016; 214:103–119. [PubMed: 27268498]

Highlights

- Pathophysiological stress induces the removal of defective mitochondria from axons
- Stressed mitochondria release SNPH cargo to enhance their retrograde transport
- SNPH cargos undergo retrograde transport en route late endosomes to lysosomes
- SNPH-mediated response is activated in the early disease stages of ALS and AD

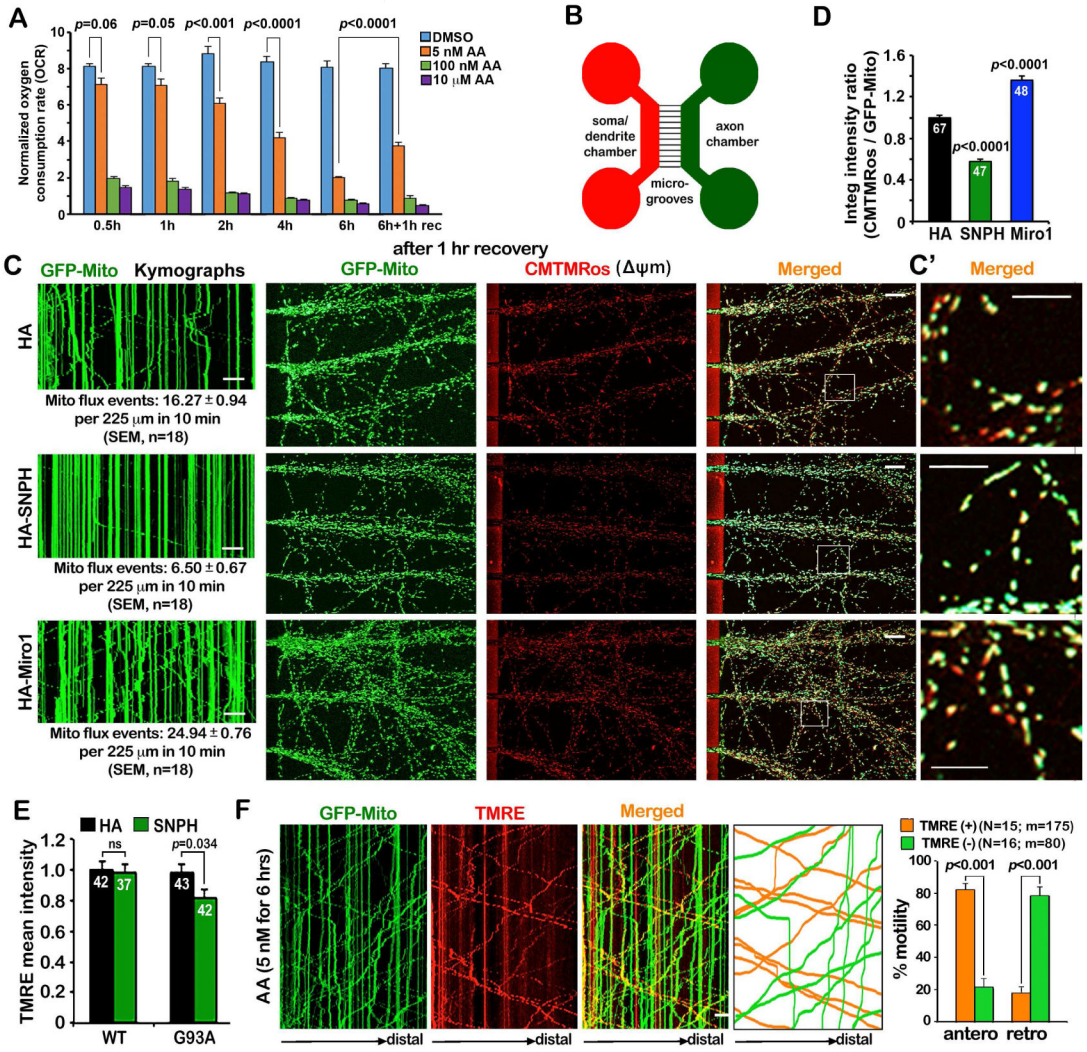

Figure 1. Arresting Mitochondrial Transport Impairs the Maintenance of Axonal Mitochondrial Integrity

(A) Seahorse XFe analysis of mitochondrial OCR following AA treatment with various dosages and durations. Cortical neurons at DIV10 were treated with DMSO or three concentrations of AA (5 nM, 100 nM, and 10 μM) for various time periods as indicated plus a 1-hour recovery following the 6-hour AA treatment. The OCR values were normalized with the cellular protein content of neuronal lysates. Note that while acute AA treatment (0.5 hours) with a high-dose (100 nM or 10 μM) causes a dramatic reduction of OCR, a low-dose AA (5 nM) gradually and reversibly reduces OCR over 6 hours (Also see Figure S1).

(B) Schematic diagram of a microfluidic chamber that allows physical and fluidic separation of axons from cell bodies and dendrites. Cortical neurons were seeded in the soma/dendritic chamber where cell bodies and dendrites are restricted, while axons grow into the axonal chamber through the microgroove channels (450 μm in length). The device permits restricted depolarization of axonal mitochondria by adding AA in the axonal chamber.

(C, D) Kymographs in the microgrooves (left panels), mitochondrial images in the axonal chamber (middle and right panels), and quantitative analysis showing that impaired the

maintenance of mitochondria $\Delta\psi_m$ in axons by arresting mitochondrial transport following 5 nM AA treatment. Cortical neurons were infected with lentivirus encoding GFP-Mito and HA, HA-SNPH, or HA-Miro1 at DIV0. At DIV8, 5 nM AA was applied to the axon chamber for 3 and 6 hours followed by a 1-hour recovery. 100 nM CMTMRos was loaded for 20 minutes before fixation and imaging of mitochondrial $\Delta\psi_m$. In the kymographs, vertical lines represent stationary mitochondria; slanted lines or curves to the left represent retrograde; to the right indicate anterograde motile mitochondria. The time-lapse images were captured for 100 frames with 5-sec intervals for 10 minutes. C′: enlarged views of the boxed regions. The relative integrated intensity ratio of CMTMRos against GFP-Mito was measured within individual mitochondria and normalized by HA control (Also see Figure S2).

(E) Arresting mitochondria motility by overexpressing SNPH impairs the maintenance of axonal mitochondrial integrity in DRG neurons isolated from adult (P40) $hSOD1^{G93A}$ mice at the early disease stages. DRG neurons were co-infected with lentivirus expressing GFP-Mito and HA or HA-SNPH. Axonal mitochondrial $\Delta\psi_m$ was analyzed at DIV7 by loading 20 nM TMRE. The average mean TMRE intensity was assessed by relative TMRE fluorescence intensity within individual GFP-Mito masked areas in axons.

(F) Kymographs and quantitative analysis showing the biased bi-directional transport of healthy versus dysfunctional mitochondria under mild stress conditions. DRG neurons were transfected with GFP-Mito at DIV0 and treated with 5 nM AA for 6 hours followed by a 1-hour recovery in fresh culture medium at DIV3. After neurons were loaded with 20 nM TMRE for 10 minutes, time-lapse images were taken in distal axons. Note that the majority of healthy mitochondria (orange), labeled with both TMRE and GFP-Mito, move in an anterograde direction toward the distal axon while depolarized ones (green) that lose TMRE staining mainly move toward the soma. The time-lapse two-channel images were captured for a total of 200 frames with 3-sec intervals.

Data were quantified from n=9 samples (A), n=18 microgrooves (C), n=47–67 axonal chamber images per condition (D), n=37–42 neurons per condition (E), the total number of organelles (m) in 15–16 axons of DRG neurons isolated from three P8–P10 rats (sex: random) (K) in three independent experiments. Data were expressed as mean ± standard error and analyzed by one-way ANOVA with post hoc testing by Tukey's multiple comparisons test (A, D, E) or the Mann-Whitney test (F). Scale bars: 20 μm (C) or 10 μm (C′, F).

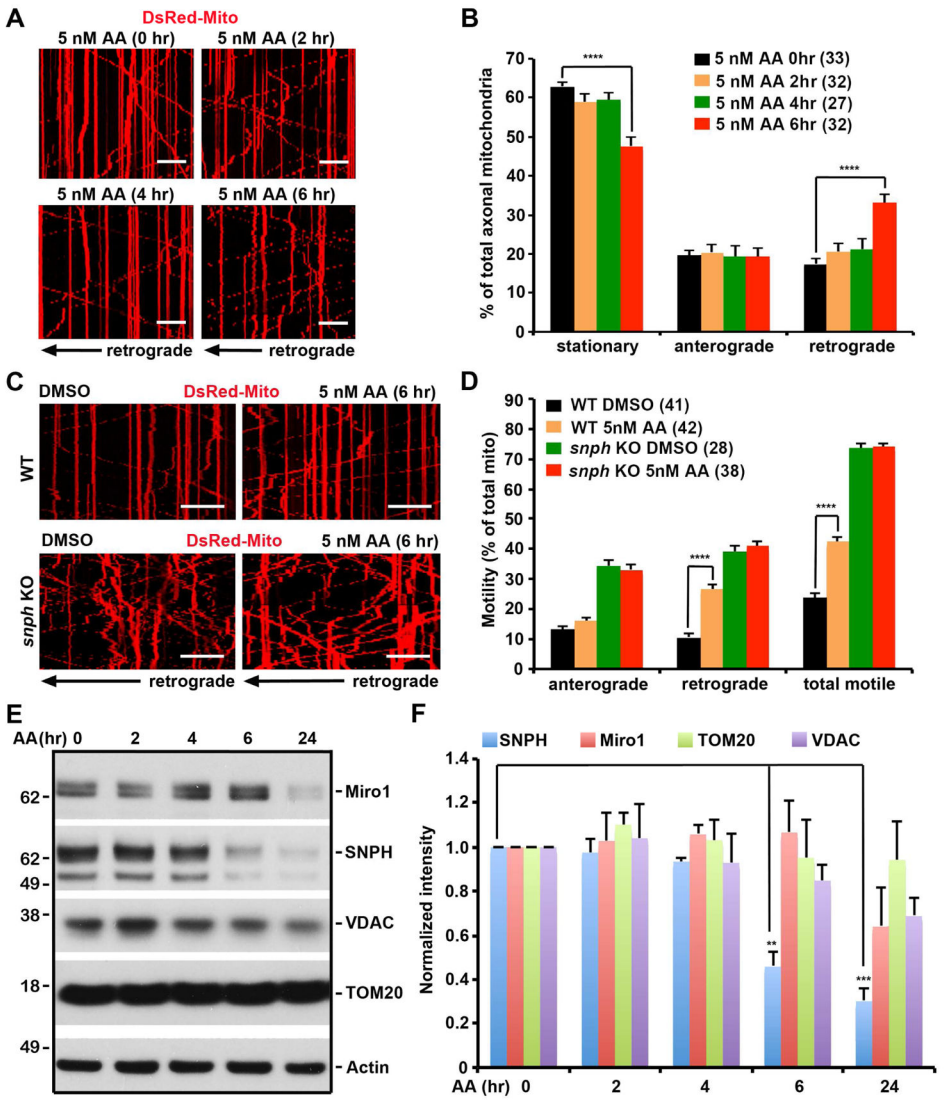

Figure 2. SNPH Mediated the Regulation of Axonal Mitochondrial Transport in Response to Mild Stress

(A, B) Kymographs (A) and quantitative analysis (B) showing enhanced retrograde transport of axonal mitochondria in response to mild stress. Hippocampal neurons were transfected with DsRed-Mito at DIV6, followed by treatment of 5 nM AA at DIV10 for various time periods as indicated. Note that axonal mitochondria remain highly motile; a 6-hour treatment with 5 nM AA selectively enhances retrograde transport (Also see Movies S1–S4).

(C, D) Kymographs (C) and quantitative analysis (D) showing a critical role of SNPH in the stress-induced regulation of axonal mitochondrial transport. Axonal mitochondrial motility of WT and *snph* KO cortical neurons was assessed before and after 5 nM AA treatment for 6 hours. Note that the AA-enhanced retrograde transport was not observed in *snph* KO neurons.

(E, F) The selective degradation of SNPH following 5 nM AA treatment. Cortical neurons at DIV10 were treated with DMSO or 5 nM AA for different time periods as indicated. Equal amounts (9 μg) of cell lysates were sequentially immunoblotted on the same membrane with

various antibodies after stripping. The intensities of OMM proteins SNPH, Miro1, TOM20, and VDAC were calibrated with actin levels and normalized to the 0-hour time point. Data were from three independent experiments.

The time-lapse images were captured for a total of 100 frames with 5-sec intervals (A, C). Data were analyzed from the total of 732–906 mitochondria in n=27–33 axons per condition (B), the number of n=28–41 axons and 673–1090 mitochondria per condition from four pairs of WT and *snph* KO littermates in four independent experiments (D). Data were expressed as mean ± standard error. Comparisons were performed by the one-way ANOVA test (B, D) or unpaired Student's *t*-test (F) (**, $p<0.01$; ***, $p<0.001$; ****, $p<0.0001$). Scale bars: 20 μm.

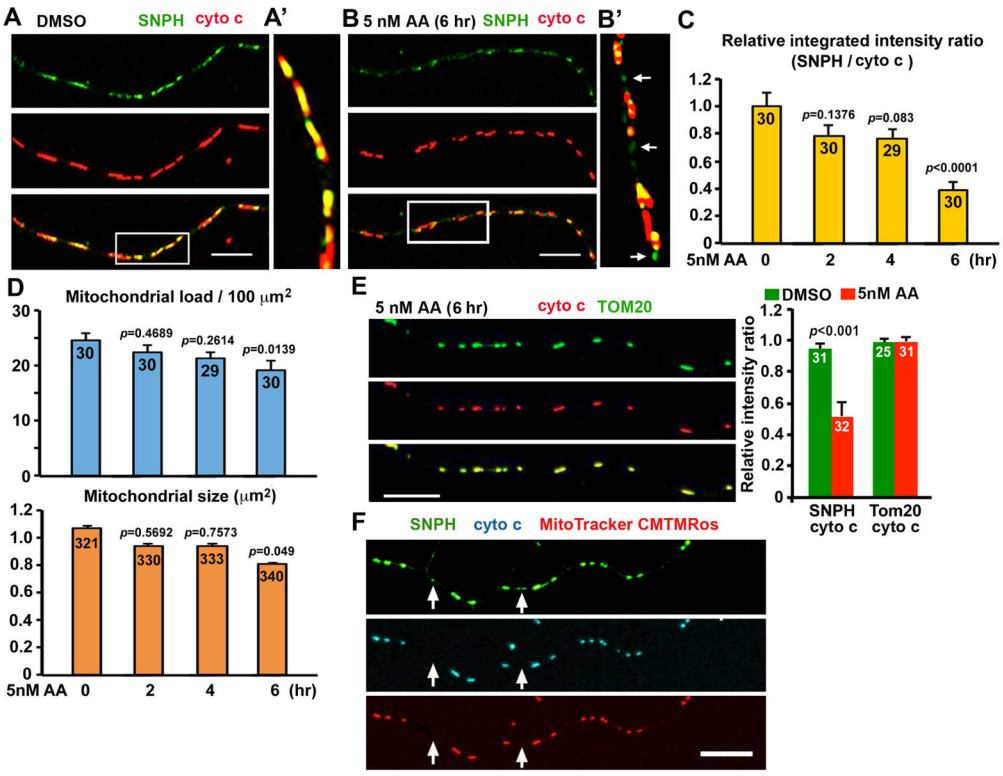

Figure 3. Generation of SNPH Cargo Vesicles from Stressed Axonal Mitochondria

(A–C) Representative images (A, B) and quantitative analysis (C) showing the generation of SNPH cargo vesicles from axonal mitochondria in response to mild stress conditions. Hippocampal neurons at DIV10 were treated with DMSO or 5 nM AA for 0, 2, 4, and 6 hours, followed by co-immunostaining with antibodies against cytochrome c (cyto c) and SNPH. Enlarged views of the boxed regions were shown in A′ and B′, respectively. Arrows indicate SNPH cargo vesicles detached from mitochondria (B′). The mean integrated intensity ratio of SNPH/cyto c was quantified following AA treatment (C). Note that normalized SNPH content (integrated intensity ratio against cyto c) was significantly reduced after a 6-hour treatment with 5 nM AA.

(D) Quantitative analysis of average mitochondrial load (summed mitochondrial area per 100 μm axon length) and mitochondrial size following the 5 nM-AA treatment.

(E) Images and quantitative analysis showing no detectable removal of TOM20 from axonal mitochondria after a 6-hour treatment with 5 nM AA (Also see Figure S3).

(F) Representative images showing the loss of cyto c and $\Delta\psi_m$ of SNPH cargo vesicles after detaching from axonal mitochondria. Hippocampal neurons were loaded with the $\Delta\psi_m$ dye CMTMRos (pseudocolored red), followed by co-staining with anti-SNPH (pseudocolored green) and anti-cyto c (pseudocolored cyan) antibodies. Arrows point to SNPH cargo vesicles (green) without cyto c and $\Delta\psi_m$.

Data were quantified from n=29–30 axons for each group (C, upper panel of D), n=321–340 mitochondria in 13–15 axons (lower panel of D), and n=25–32 axons for each group (E) in three independent experiments. Data were expressed as mean ± standard error. Comparisons were performed by one-way ANOVA (C, D) and Mann-Whitney test (E). Scale bars: 10 μm.

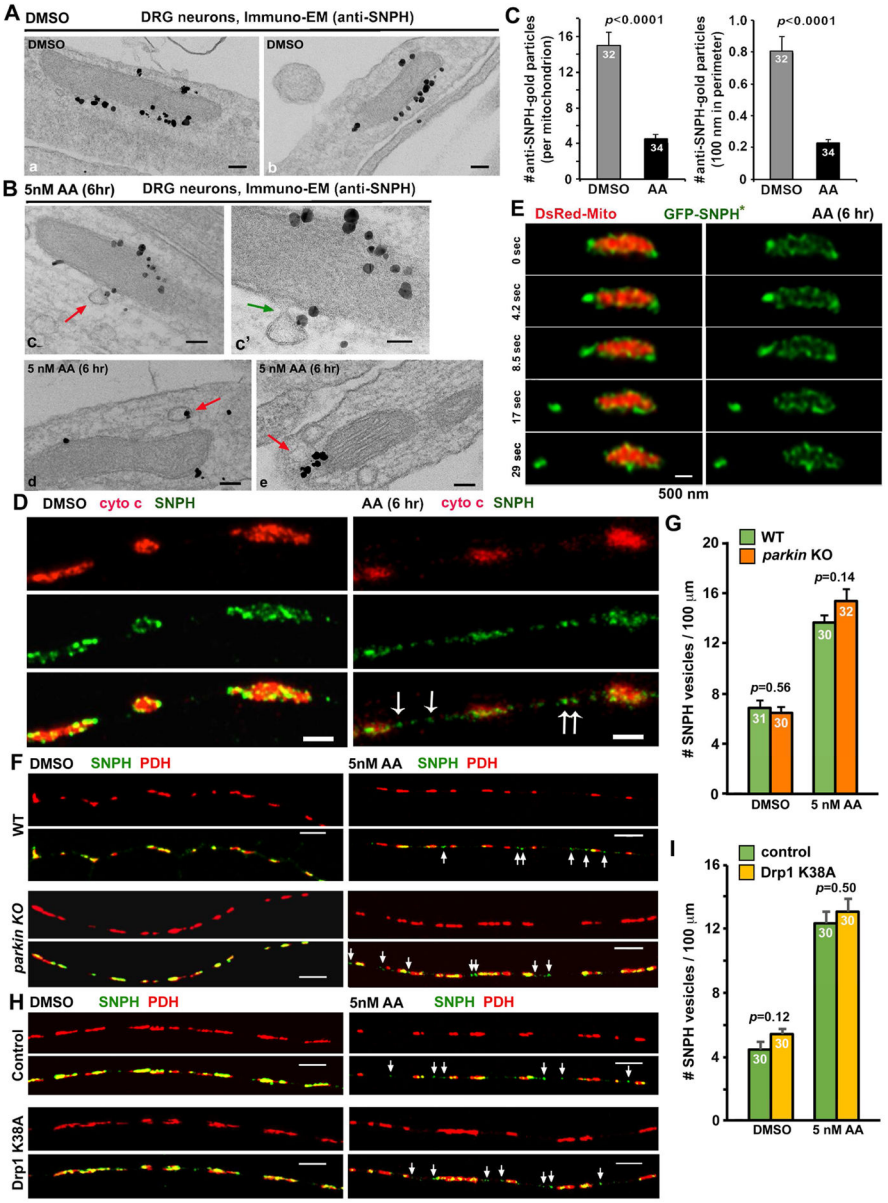

Figure 4. The Parkin- and Drp1-Independent Budding Process of SNPH Cargo Vesicles from Axonal Mitochondria

(A, B) Immuno-EM graphs showing the budding process of SNPH in the form of cargo vesicles. DRG neurons were treated with DMSO (A) or 5 nM AA for 6 hours (B) at DIV3 and labeled with an anti-SNPH antibody and nanogold conjugates. SNPH-gold particles outline the surface of mitochondria (a, b) under DMSO control conditions or are present at the limiting membrane of a budding vesicle that is continuous with the OMM (c, c′) or single-membrane vesicular structures (d, e) in close proximity to mitochondria following AA treatment. c′: an enlarged view of a budding SNPH cargo. Arrows point to SNPH vesicles.

(C) Quantitative analysis showing reduced SNPH-gold particles associated with the OMM under the AA-induced stress condition compared to DMSO control.

(D) STED images showing endogenous SNPH cargo vesicles (arrows) detached from axonal mitochondria in response to AA-induced stress. DRG neurons were treated with DMSO or 5 nM AA for 6 hours at DIV3, followed by co-immunostaining of SNPH and cyto c.
(E) Time-lapse STED live images showing a SNPH cargo vesicle pinching out from an axonal mitochondrion. DRG neurons at DIV0 were transfected with DsRed-Mito and GFP-SNPH* and imaged at DIV3 after a 6-hour incubation with 5 nM AA. Note that GFP-SNPH* (green) first appears as puncta on the surface of the mitochondrion. Under mild stress conditions, a SNPH cargo vesicle leaves from stressed mitochondrion in a time scale of 4–8 seconds.
(F, G) Images (F) and quantitative analysis (G) showing Parkin-independent generation of SNPH cargo vesicles. Mouse DRG neurons from wide type (WT) and *parkin* KO mice were treated with DMSO or 5 nM AA for 6 hours at DIV3, followed by co-immunostaining of SNPH and PDH, a mitochondria matrix marker. White arrows indicate SNPH vesicles.
(H, I) Images (H) and quantitative analysis (I) showing Drp1-independent generation of SNPH cargo vesicles. DRG neurons were transfected with a control vector or Drp1 K38A mutant at DIV0 and treated with DMSO or AA (5 nM for 6 hours) at DIV3, followed by co-immunostaining of SNPH and PDH. White arrows indicate SNPH vesicles.
Data were analyzed from the total number of immuno-EM graphs (C) from four P8–10 rats (sex: random) or the total number of axons (G, I) indicated within the bars from three experiments (G: three pairs of P90 mice; I: from three P8–10 rats, sex: random). Error bars: SEM. Unpaired student's *t*-test with Welch's correction. Scale bars: 100 nm (A, Ba–e), 50 nm (Bc′), 1 μm (D), 500 nm (E), and 5 μm (F, H) (Also see Figure S4).

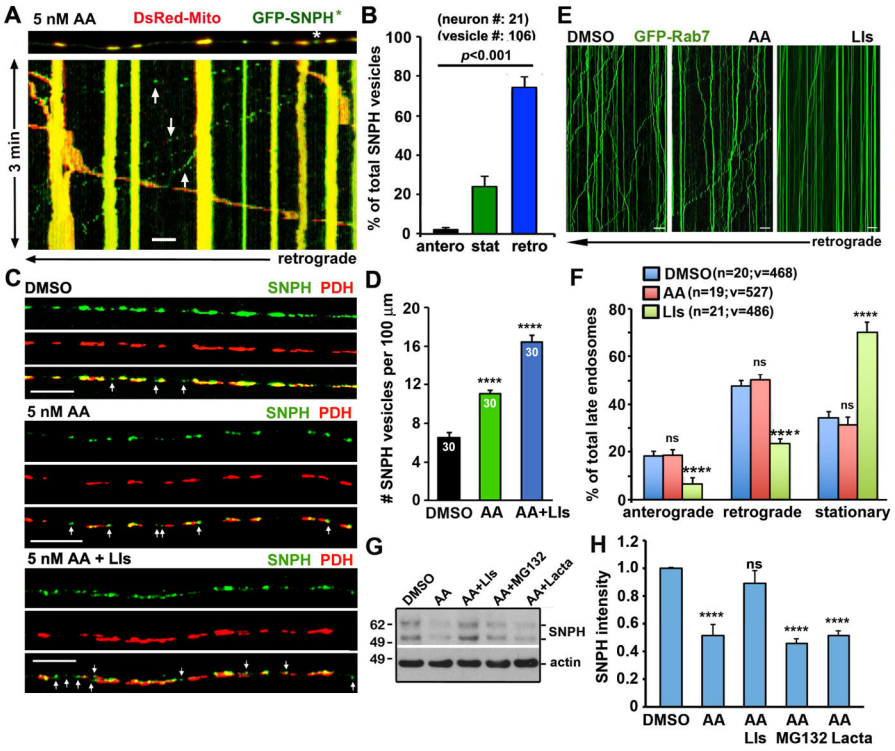

Figure 5. SNPH Cargo Vesicles Undergo Retrograde Transport for Lysosomal Degradation

(A, B) A representative image and kymograph (A) and quantitative analysis (B) showing retrograde transport of SNPH cargo vesicles. DRG neurons were transfected with GFP-SNPH* and DsRed-Mito at DIV0 and treated with AA (5 nM for 6 hours) at DIV3, followed by dual-channel time-lapse imaging at 2-second intervals for a total of 3 minutes. The upper panel shows the first frame of the time-lapse series. The asterisk points to a SNPH cargo vesicle (green) and the yellow organelles represent mitochondria (DsRed-Mito) containing GFP-SNPH*. Data were collected from 21 neurons with total of 106 vesicles from three P8–P10 rats; sex: random.

(C, D) Images (C) and quantitative analysis (D) showing the reduced turnover of SNPH cargo vesicles after inhibition of the endo-lysosomal pathway. DRG neurons were treated with DMSO or AA (5 nM for 6 hours) in the presence or absence of lysosomal inhibitors (LIs) (10 μM: pepstatin A, leupeptin and E64D), followed by co-immunostaining of SNPH and PDH. Data were collected from 30 neurons examined for each group from three P8–P10 rats; sex: random. Arrows point to SNPH cargo vesicles.

(E, F) Kymographs (E) and quantitative analysis (F) showing impaired retrograde transport of LEs in axons treated with LIs. DRG neurons were transfected with GFP-Rab7 at DIV0 and treated with AA or LIs. Note that LIs impair the LE motility in axons. The total number of LEs (v) in the total number of axons (n) examined is indicated in parentheses from at least three experiments. Data were collected from the total of vesicles (v) in the number of neurons (n), as indicated, from three P8–P10 rats; sex: random.

(G, H) Immunoblots (G) and quantitative analysis (H) showing lysosome-dependent SNPH degradation. Cortical neurons at DIV10 were treated with DMSO, 5 nM AA, or 5 nM AA with LIs (10 μM E64D and 10 μM pepstatin A) or a proteasome inhibitor (10 μM MG132 or

10 μM lactacystin) for 6 hours. 10 μg of neuronal lysates were loaded and sequentially immunoblotted on the same membrane with antibodies against SNPH and actin. Note that LIs, but not a proteasome inhibitor, abolishes AA-induced degradation of SNPH. Data were collected from n=3 independent replications.

Data were analyzed with Ordinary one-way ANOVA (ns, not significant, ****, $p<0.0001$). Error bars: SEM. Scale bars: 10 μm.

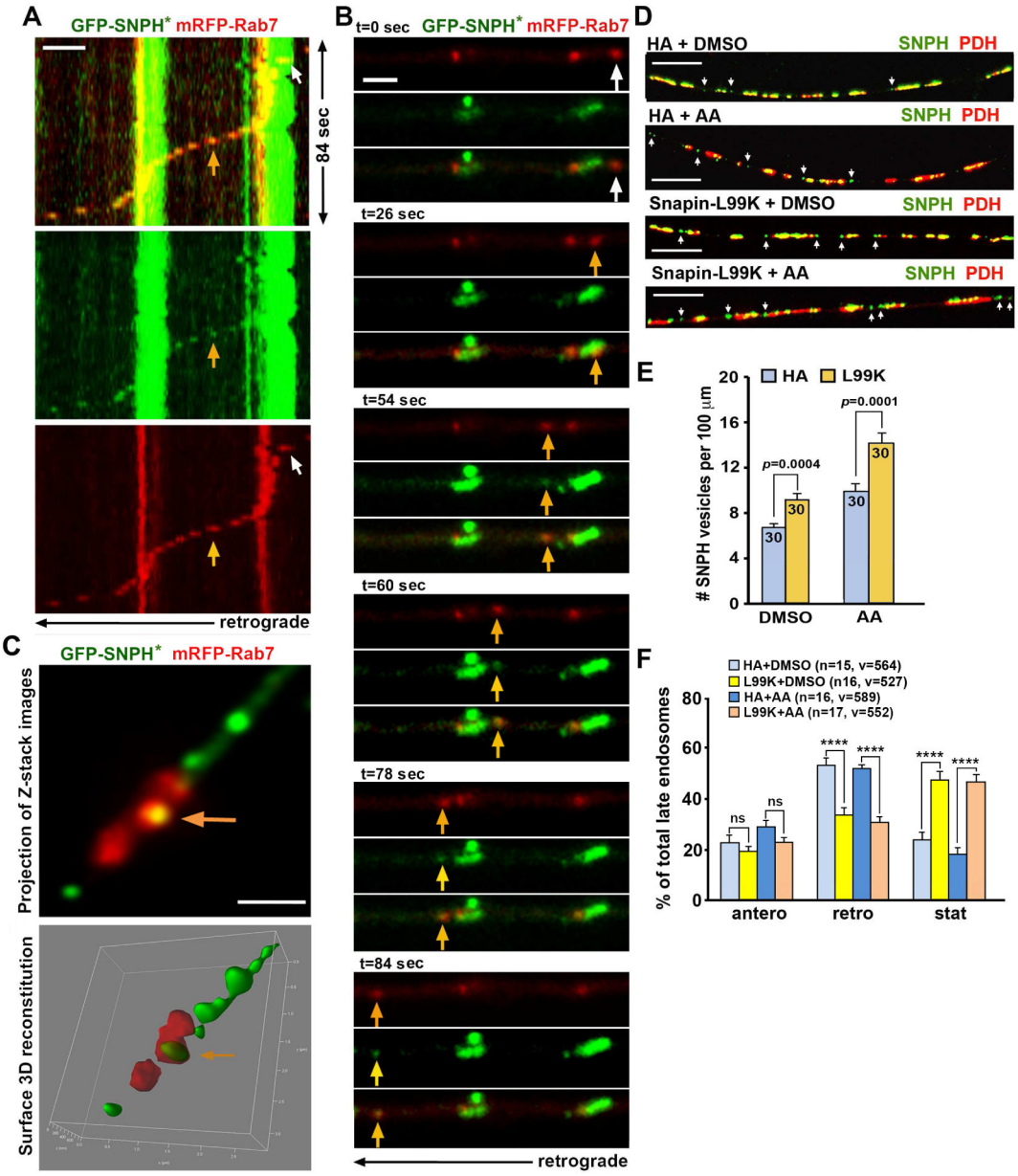

Figure 6. SNPH Vesicles Share the Ride with Late Endosomes

(A, B) Kymographs (A) and time-lapse images (B) demonstrate that a LE (red) carries a SNPH cargo vesicle (green) for retrograde transport along an axon. DRG neurons were transfected with GFP-SNPH* and mRFP-Rab7 at DIV0 and treated with AA (5 nM for 6 hours) at DIV3. White arrows indicate a LE just passing a stationary mitochondrion, whereas yellow arrows point to a newly generated SNPH cargo vesicle that rides on the LE moving in the retrograde direction toward the soma, a process that occurs within ~84 seconds (Also see Figure S5).

(C) STED image showing co-localized LE and SNPH cargo vesicle. Z-stack images were taken at step size of 110 nm. The yellow arrow indicates a SNPH vesicle (green) being

wrapped by a LE (red). The images were processed with de-convolution before max-projection and 3D surface reconstitution, respectively (Also see Movie S5).
(D–F) Representative images (D) and quantitative analysis (E, F) showing retained SNPH cargo vesicles in axons when LE transport is impaired by expressing Snapin-L99K. DRG neurons were transfected with Snapin-L99K or HA vector at DIV0 and treated with AA (5 nM for 6 hours) or DMSO at DIV3, followed by co-immunostaining of SNPH and PDH (D, E) or co-transfected with mRFP-Rab7 followed by time-lapse imaging (F). Arrows point to SNPH cargo vesicles.
Data were analyzed from a total number of axons indicated in the bars (E) or a total number of LEs (v) from the number of neurons (n) indicated in parentheses (F) in at least three experiments. Three (F) or four rats (D, E) at age of P8–P10 were used (sex: random). Unpaired *t* test (E) or one-way Anova test (F) (****: $p<0.0001$). Error bars: SEM. Scale bars: 2 μm (A, B); 1 μm (C), and 10 μm (D).

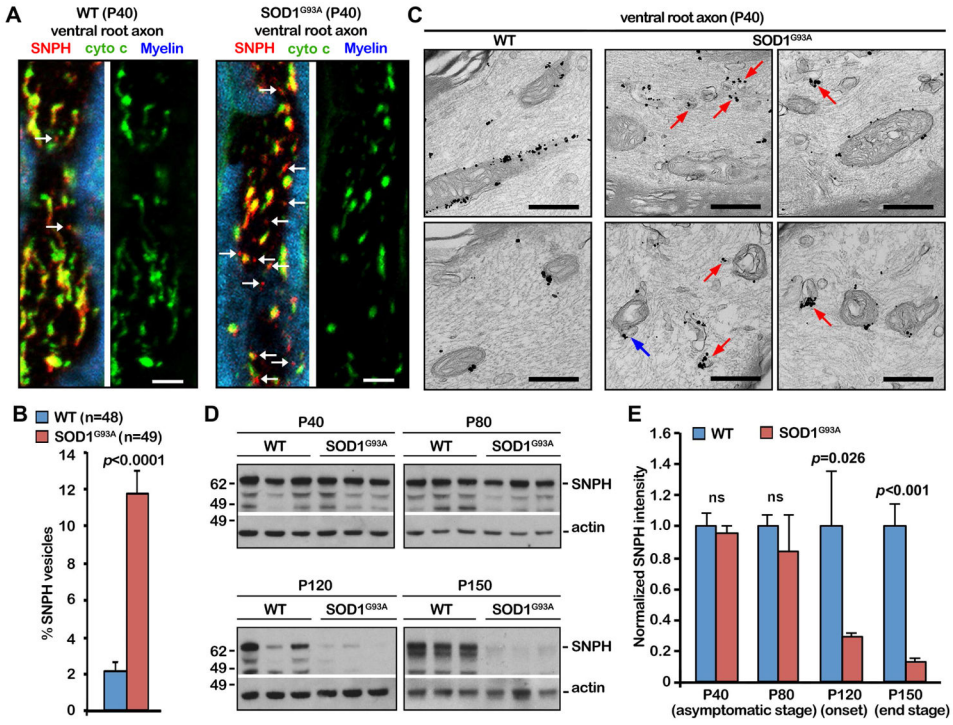

Figure 7. SNPH Pathway is Activated in Early Disease Stages of fALS-Linked Mice

(A, B) Images (A) and quantitative analysis (B) showing the bulk release of SNPH in the form of cargo vesicles from damaged mitochondria in early asymptomatic hSOD1^{G93A} mice. Ventral root axon bundles of spinal motor neurons from P40 WT and hSOD1^{G93A} littermates were co-immunostained with cytochrome c (green), SNPH (red), and Myelin dye (blue). Arrows point to SNPH cargo vesicles. SNPH vesicles were quantified as the percentage of SNPH vesicles from a total number of mitochondria labeled with both cytochrome c and SNPH. Data were analyzed from the total number of axon sections (n) from three pairs of WT and hSOD1^{G93A} littermates. Fifteen to seventeen sections were taken from each animal.

(C) SNPH immuno-EM graphs showing SNPH cargo vesicles in the ventral root axons of early asymptomatic hSOD1^{G93A} mice (P40). Red arrows point to vesicular structures labeled with SNPH-nanogold particles. The blue arrow indicates a SNPH vesicle that is pinching out of a mitochondrion.

(D, E) Western blots (D) and quantitative analysis (E) showing SNPH depletion in the sciatic nerve of hSOD1^{G93A} mice after disease onset at age P120. SNPH intensities were normalized by actin and compared with an age-matched control group. For each time point, data were collected from at least three animals (n=3) for each genotype.

Data were expressed as mean ± SEM with the unpaired Student's *t*-test. Scale bars: 10 μm (A) and 500 nm (B) (Also see Figure S6).

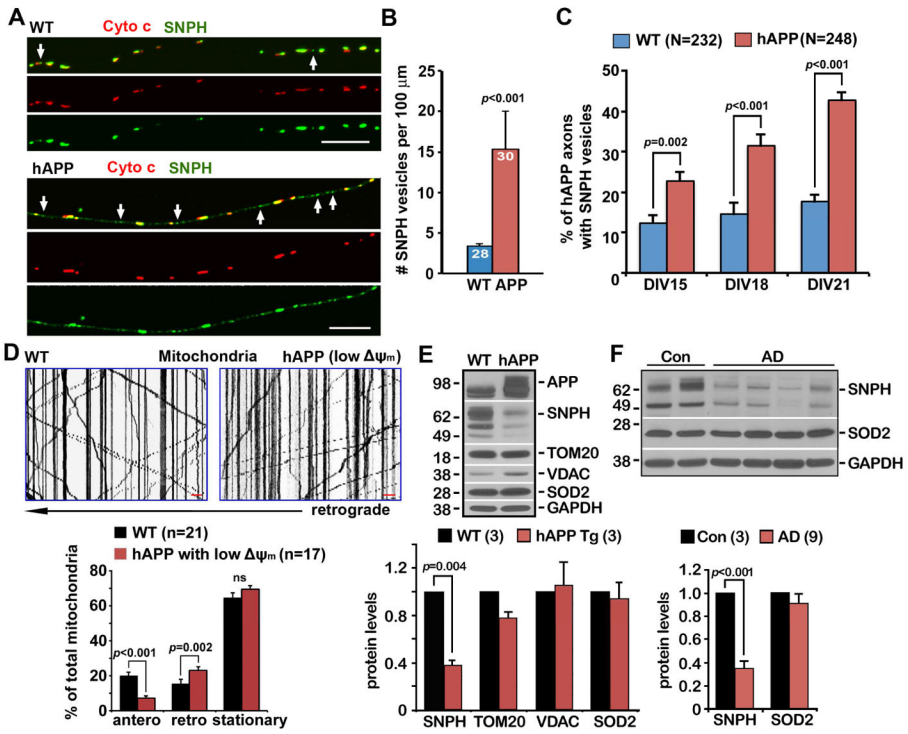

Figure 8. SNPH Pathway is Activated in AD-linked Mutant hAPP Tg Neurons

(A, B) Representative images (A) and quantitative analysis (B) showing increased generation of SNPH cargo vesicles in cortical neurons at DIV14–15 from mutant hAPP Tg (J20) mice. The average number of SNPH cargo vesicles (white arrows) per 100 μm axons was quantified from the total number of WT and hAPP neurons indicated in the bars (B) from three pairs of littermates in three independent experiments.

(C) The percentage of mutant hAPP axons with detectable SNPH vesicles. Data were analyzed from the total number of axons indicated in parentheses in three independent experiments.

(D) Representative kymographs and quantitative analysis showing reduced anterograde and enhanced retrograde transport of axonal mitochondria with reduced $\Delta\psi_m$. Data were analyzed from the total number of axons indicated in parentheses in three independent experiments.

(E) Representative western blots showing SNPH depletion in the brains of mutant hAPP Tg (J20) mice. A total of 20 μg of brain homogenates from WT and hAPP Tg mice was sequentially detected on the same membrane. Relative protein levels were normalized by GAPDH and to that of WT littermates. Data were analyzed from three pairs of WT and hAPP Tg littermates.

(F) Western blots showing reduced SNPH in postmortem brain specimens from AD patients. A total of 20 μg of brain homogenates from the cortices of age-matched controls and AD patients was sequentially detected on the same membrane. Relative protein levels were normalized by GAPDH and to those of control subjects. Data were analyzed from the number of human brain samples indicated in parentheses in three independent experiments.

Data were expressed as mean ± SEM with the Mann-Whitney test (A, D), the unpaired Student's *t*-test (B), or the two-tailed Student's *t*-test (E, F). Scale bars (A, D): 10 μm.